12-2018

Boron Nitride Thin-Film Deposited by RF Magnetron Sputtering

Jesus A. Valladares Gonzalez
The University of Texas Rio Grande Valley

BORON NITRIDE THIN-FILM DEPOSITED BY RF MAGNETRON SPUTTERING

A Thesis

by

JESUS A. VALLADARES GONZALEZ

Submitted to the Graduate College of
The University of Texas Rio Grande Valley
In partial fulfillment of the requirements for the degree of

MASTER OF SCIENCE IN ENGINEERING

December 2018

Major Subject: Electrical Engineering

BORON NITRIDE THIN-FILM DEPOSITED BY RF MAGNETRON SPUTTERING

A Thesis

by

JESUS A. VALLADARES GONZALEZ

COMMITTEE MEMBERS

Dr. Hasina Huq

Chair of Committee

Dr. Yoonsu Choi

Committee Member

Dr. Yong Zhou

Committee Member

December 2018

ABSTRACT

Valladares González, Jesus A., Boron Nitride Thin-Film Deposited by RF Magnetron Sputtering. Master of Science (MS), December, 2018, 61 pp, 2 Table, 32 figures, references, 49 titles.

Cubic Boron Nitride is considered a superhard material, its thermochemical stability makes it suitable for applications with corrosive environments and high temperatures. C-BN is grown by PDV on Si substrates. The plasma is energized via an RF source to sputter the target. The ion species in the plasma can be described by the classic electrodynamic expression $\ddot{x} = qE/m$. Plasma temperature is given by T = (6.2836*E/8*k). The sputter is given by the ratio of the heat transfer to the enthalpy of formation ΔH_f°, of the target. The Hall Measurement is performed as recommended by NIST. The measurement was performed on a c-BN thin film deposited on a Si substrate. The deposition was done at 6mT, 600°C, 6Ar/9N_2, for 18 Hr. The voltage polarity measurement indicates that holes are the majority charge carrier and verifies the p-type conductivity of the sample, this is an important parameter in semiconductor devices.

DEDICATION

The completion of this graduate work would have not been possible without the support of my family and friends throughout the years. My Wife, Tania Diaz, my father, Alejandro Valladares II, my mother, Nely Gonzalez, my brother, Alejandro Valladares III, my sister, Laura Valladares, my brother, Daniel Valladares, my colleague, Juan Hermosillo, my friend, Carlos Maurilio, have always inspired and provide motivation. Thank you for all you do.

ACKNOWLEDGEMENTS

I'll always be grateful to Dr. Hasina Huq, chair of my dissertation committee, for the past years of guidance and patience that allowed me to gain experience and perspective in a professional, scientific, and personal ways. Thanks to my dissertation committee members: Dr. Yoonsu Choi, and Dr. Yong Zhou who've reviewed the material and provide a direction in the different fields of work.

I would also like to thank my colleagues at UTRGV who helped getting familiar with the laboratory procedures and aided in experimental data collection for the spectroscopy and microscopy portions of the study.

TABLE OF CONTENTS

Page

LIST OF TABLES

Page

LIST OF FIGURES

Page

CHAPTER I

INTRODUCTION

This work goes over some very common semiconductor material properties and Physical Vapor Deposition (PVD) method of the Radio Frequency Magnetron Sputtering System (RF-MSS). The detailed discussions of the properties of metals, insulators, and semiconductors can be found elsewhere in semiconductor and solid-state physics texts. The MSS on the other hand is not very well understood. Although it's use is wide in a variety of industries that go from construction to the wafer fabs. The MSS [3][4][42][46] uses a plasma to evaporate a target material and grow a thin film over a substrate.

Most of the work dealing with plasms has been done for the study of nuclear reactors, distant cosmic phenomena e.g. stars, or some that are closer in distance such as the aurora boreal. There has also been a large amount of effort dealing with arc or coronal discharges, especially in high voltage applications since they are unavoidable yet undesired effect in power lines. These works still need to be translated to the PVD process to fully understand its limitations and design optimum materials in the future. In this work a model for the PVD sputtering is developed and the resulting material is tested with known electrical testing standards for carrier mobility and concentration.

CHAPTER II

SEMICONDCUTOR DEVICES

Faraday's developments in electromagnetism are commonly regarded as the birth of what is now perceived as modern electric devices, however, the beginning of commercialized semiconductor devices can be traced back to Braun's experiments on the galena crystal (lead sulfide), [31] Braun observed a variable electrical resistance with a change in current, the device developed on these experiments was known as the "crystal detector". Figure 2.1 shows a modern crystal detector from Keysight Technologies with an SMA to BNC adapter. However, the detector was quickly replaced by vacuum tube technology due to device reliability. Semiconductor materials are and remain an active area of research.

Figure 2.1 - Modern Diode crystal detector from Keysight Technologies

Figure 2.2 - Thermionic Valve Diode, https://www.electronics-notes.com/articles/history/vacuum-tube-thermionic-valve/history.php

The elements as presented in the Periodic table are grouped to have common features, e.g. the number of electrons in the outer shell. Metals tend to have a low electric resistance which is why they're commonly used as electric conductors, while noble gases tend to be chemically stable, some compounds commonly used as dielectrics and insulators include SF_6 in waveguide systems, or SiO_2 in electronic devices and circuits. Figure 2.3 shows the structure of a Metal Oxide Field Effect Transistor (MOSFET) with the oxide portion acting as an electric insulator.

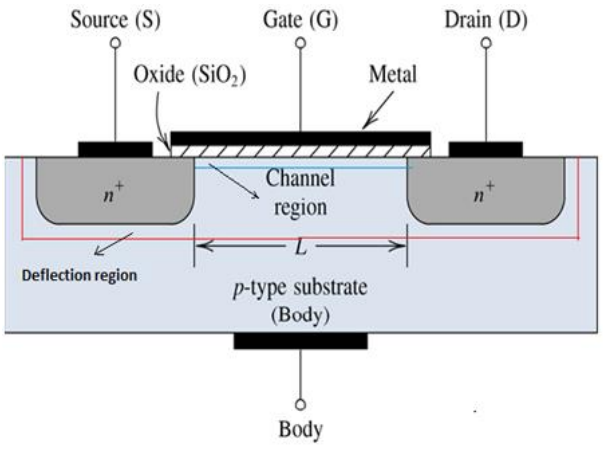

Figure 2.3 - Diagram of MOSFET structure showing the Si Oxide region acting as insulation in the Gate electrode, https://www.elprocus.com/mosfet-as-a-switch-circuit-diagram-free-circuits/

The basic materials used in electronic devices belong to a special class known as Semiconductors (most of the metalloids in the familiar periodic table of elements). Although metals and oxides are also used for device fabrication and functionalization. Semiconductors can have their behavior altered to become electric conductors, insulators, or a variable resistance, e.g. under an applied electric field, a semiconductor can go from electrically insulating to conducting and vice versa, depending on a variety of parameters such as chemical purity and the applied fields. These effectively change the electrical resistance, and can produce electric switches, amplifiers, sensors, among other device applications. All these normally happen in a plethora of highly specialized manufacturing processes that will not be discussed here as this work focuses on the RF MSS (Radio Frequency Magnetron Sputtering System) for PVD (Physical Vapor Deposition).

Fabrication of modern electronics devices depends on modern techniques. Much work needs to be done to overcome current technological challenges. These challenges may be

overcome by a better understanding the thermochemical processes used in the fabrication process, and the use of novel alloys as compound semiconductors [5][7].

Figure 2.4 below shows a simple electric circuit with a resistor on (a), an insulator on (b), and an unknown on (c). The unknown values here refer to the variable electric properties of the semiconductor sample.

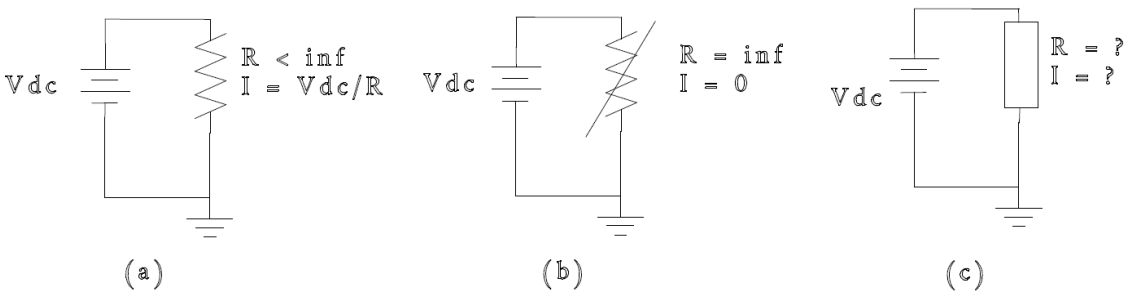

Figure 2.4 - (a) conductor with finite resistance R, (b) insulator with infinite resistance, (c) Semiconductor material with variable properties.

Some common devices fabricated using these semiconductors are diodes and transistors, resistors and LEDs (Light Emitting Diode), etc. The transistors can be FET or bipolar devices. Advancement of these technologies is of essence for today's economic and technological challenges because semiconductor devices are the basic components of the microprocessor technology in modern computers, display and sensing technology. The modern diode (or rectifier) works based on the chemical potential difference at the contact between a p-type and n-type semiconductor. With the type being the determined by the majority charge carrier, and where n-type implies that occupied density of states of the negative charge carrier (the electron) in the conduction band is greater than that of the positive charge carriers (holes). In n-type

materials, electron flow makes most of the contribution to the total electric current. Holes are the main charge carriers in p-type materials.

This is an oversimplification for any semiconductor topic, whether it be materials or devices. A more complete explanation requires a more detailed description of the electron as a subatomic particle and how the electric charge carrier moves inside of solids. This must be accompanied by a description of crystal lattices and quantum mechanics. Electrons in atoms only exist in allowed energy levels (i.e. electron orbitals) these can be described in detail by solving Schrodinger's equation for the corresponding energy levels for the electron in the material species conduction band.

A detailed description of semiconductor materials properties and behavior is not covered here as it is found in multiple solid-state physics and semiconductor devices texts. It is worth to mention however, the difference in the conduction and valence band that makes the most commonly referred difference between conductors, insulators, and semiconductor materials. In a semiconductor the valence and conduction band are separated by what is referred to as the forbidden band, this is a region that cannot be occupied by the electron in the solid. In an insulator, the conduction band is too wide, such that the probability for a charge carrier to contribute to conduction is zero. In conductor, such as most metals, the valence and conduction bands overlap, such that charge carriers are always available for conduction. The forbidden region is the difference between the conduction mand and the valence band and it is commonly referred to as the Energy Band Gap E_g.

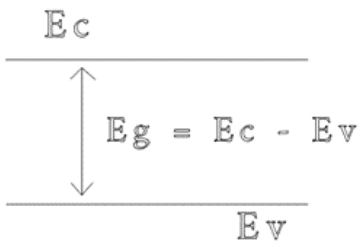

Figure 2.5 - Semiconductor Energy Band Gap Diagram

The energy band refers to the quantized nature of the subatomic particles, such as the electron, and the fact that in the atom, it can only exist in specific energy states, the energy gap for a given semiconductor is shown in Figure 2.5, with E_v being the edge of the valence band and E_c for the conduction band. The core electrons do not contribute to the conduction process, and it is only the valence electrons that are included in these assumptions (although core electrons obey the same physical laws). The energy band gap is a measure of how much energy is necessary for a charge carrier to escape the valence band and go into the conduction band (leaving a hole behind) thus being able to contribute to the conduction process. The amount of charge carriers available for conduction (the occupied density of states) is a function of temperature. Because of this, no charge carriers are available at absolute zero. This also means that semiconductor devices become functionally unstable at relatively high temperatures. Figure 2.6 below shows a block diagram of the MOSFET without and with an applied bias showing the conduction channel generation that forms the basis of operation of today's modern switching and computing devices. Figure 2.7 shows the increased transistor density in a single chip through time as per Intel Corp devices.

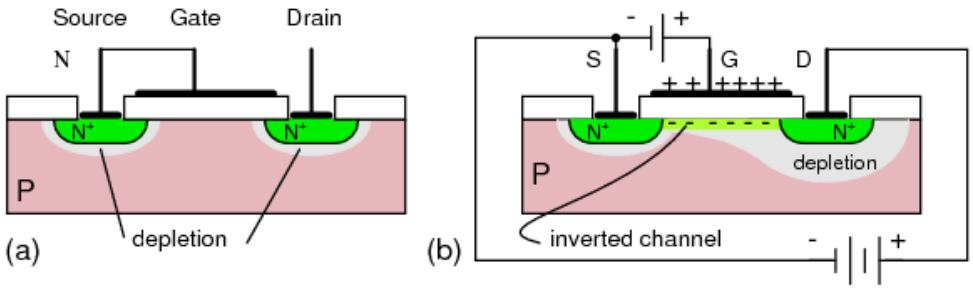

Figure 2.6 - a) block diagram of MOSFET structure, b) biasing and conduction channel generation in MOSFET device https://www.allaboutcircuits.com/textbook/semiconductors/chpt-2/insulated-gate-field-effect-transistors-mosfet/

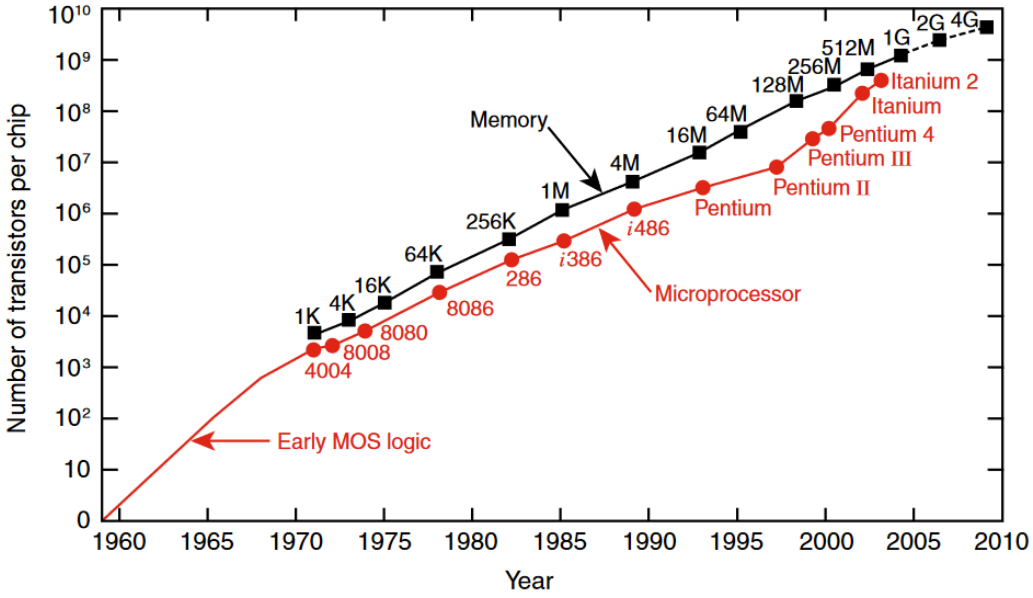

Figure 2.7 – Moore's Law reflecting the Exponential growth in density on a single chip (Intel Corp trademarks), Harry K., Charles Jr. Miniaturized Electronics, John Hopkins Apl Technical Digest, 2005

CHAPTER III

SEMICONDUCTOR MATERIALS

Silicon (Si) is the 14th element from the periodic table, it belongs to group 4A along with Carbon (C), Figure 3.1 below is a model of the electronic shell structure of the Si atom. Si has been the choice for semiconductor applications for decades since the interest in electronics components couldn't be satisfied by vacuum tube technology. Electronics devices, however keep getting smaller, faster, and there is an increasing demand for high power density. This miniaturization is accompanied with a demand for more extreme physical characteristics, such as high temperature operation tolerance and thermochemical stability.

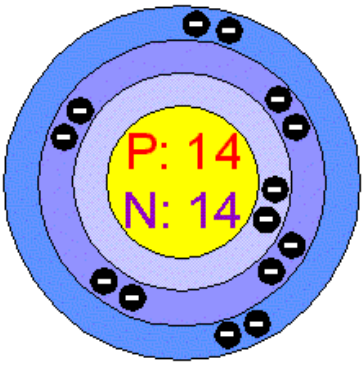

Figure 3.1 - Electronic Shell model of the Si atom, http://www.chemicalelements.com/elements/si.html

Some alloyed materials show properties that exceed that of ones currently in sue, i.e. when compared to those of Silicon. While Si is commonly used because it proved easier to work

with. Among the materials of interest are Boron Nitride (BN), Aluminum Nitride (AlN), Gallium Nitride (GaN), and Indium Nitride (InN). Group III-V compound semiconductors exhibit extreme properties when compared to those of Si, e.g. the melting point of BN is much higher than that of Si at standard pressure, i.e. cubic BN is thermochemically stable up to 3246 K Vs 1685K of Si at 1 Atm of pressure. At the same time, its Energy Bandgap and thermal conductivity are much higher than Si. These properties make BN a candidate for High Power and thermal management applications. The cubic phase of BN (c-BN) has relative dielectric permittivity $\varepsilon_r = 7$. High permittivity is desired in many applications such as Radio Frequency design, reflectors, and dielectric substrates, this also makes it a good candidate for new battery and capacitance technology.

BORON NITRIDE

Boron Nitride [20] does not occur in nature. It can be synthesized in different crystalline forms. The most commonly researched are the hexagonal wurtzite, hexagonal graphite form, and the zinc-blende or cubic form, w-BN, h-BN, and c-BN respectively. All these forms constitute different thermochemical phases with different mechanical, thermal, and electric properties. The focus of this work is to examine the properties of c-BN synthesized by the PVD process since the group III-V semiconductor is considered a super hard material, and it is found to grow as a thin film on Si substrates via Physical Vapor Deposition by Radio Frequency Magnetron Sputtering of a hexagonal Boron Nitride target. The wurtzite and zinc-blende crystal structures are shown in a diagram form in Figure 3.2.

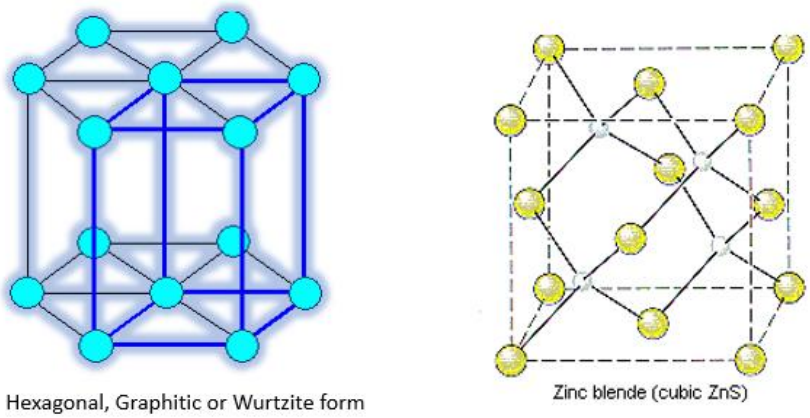

Figure 3.2 - Wurtzite crystal structure (left), Cubic Zinc Blende (right), figures accesible at http://chemed.chem.purdue.edu/genchem/topicreview/bp/ch13/unitcell.php

Material hardness [1] is defined as the material's resistance to deformation. The bulk modulus (bulk material resistance to compression), and the sheer modulus (the material resistance to being indented) are common measures of the hardness of the material in question. Conditions for a material to be considered hard [12] are; that it is not easily compressed under pressure, and that stress in any given direction will not be transmitted along any other direction. It is mentioned that covalent bond networks "fulfill this requirement" as the bonds are highly directional and not easily deformable. Diamond (the cubic form of carbon) is one of the hardest materials known, it has a bulk modulus ~ 450 GPa, c-BN ~ 370 GPa. Note that bulk modulus has the unit of pressure. Other semiconductor materials that can be considered for their hardness due to being close in order of magnitude are; SiO2, SiC, Al2O3, AlN, etc. It is also noted that the bond length is inversely related to the hardness of the material. E.g. the bond length for C-C bond is of 1.54 Å Vs. 1.57 Å of c-BN, where both are fully covalent crystal structures. The bond length in c-BN [1] [2] is roughly less than half of the lattice constant, $a = 3.5$ Å.

PROPERTIES OF CUBIC BORON NITRIDE

The cubic phase of Boron Nitride (Borazon) is not found in nature and is was first synthetized by Robert H. Wentorf, in 1957, at the GE Research Laboratory in Schenectady, NY. This was achieved by “extremely high pressure and temperature” [13]. This is in accordance with phase diagrams available for its synthesis, which indicate an extremely high formation energy. As discussed next, BN is currently under research and development for electronic applications and the text presents some examples of how it has been used for specific applications, note that this is not an extensive list nor a survey of the current state of research.

The electric conductivity is analogous to the expression of heat transfer expression. Experimental values of the thermal conductivity of bulk c-BN is found to be [2] 7.4 W/(cm*C), while Silicon has a thermal conductivity of [3] 1.3 W/(cm*C). The comparison rises interest in research on c-BN. Applications that go beyond electronic components include electric insulators, these range from the ones commonly used in the electric utilities to electronic component design, high power equipment and high frequency switching. The thermal conductivity of materials indicates the rate at which thermal energy is transferred from one piece of material to another, assuming there is a good thermal contact between the two. The unit for thermal conductivity expressed in Watts/(meter*C). Materials with low and high thermal conductivity are commonly used as thermal conductors or thermal insulators respectively. In addition to the high thermal conductivity, BN is known to be thermochemically stable at a wide range of temperatures and pressures. This is a desirable characteristic for chemical and biological sensing applications.

Polyethylene is commonly used as a thermal and electric insulator. Commercial polyethylene shows values for thermal conductivity of 0.52 W/(cm*C). The low thermal

conductivity value can lead to thermal accumulation and lead to equipment failure. In, the proper mixture of BN grains inside a polyethylene insulator filling allows to isotopically increase the insulator's thermal conductivity. This results in a decrease in the thermal accumulation and an increase in the surface of the material resistance to arching. The authors present an SEM image of the surface of the pure polyethylene Vs. the insulator BN mixture [48] where there is an apparent structure formation due to the crystallite nature of the BN grains. Although the authors mention the use of different grains sizes, in the micro $10^{-6}m$, and nanometer ($10^{-9}m$) range there is no mention of other physical characteristics of interest e.g. crystal structure and electric conductivity. The text also reports on an increase in the relative permittivity with an increase of BN concentration in the BN/Polyethylene mixture. Known crystal forms of BN have a high dielectric permittivity. This might be useful in switched power applications employed in high-power density applications. Noting that because of the Wide-Band-Gap of c-BN, it is expected to act as an insulator at room temperature and relatively low electric fields, but the occupied density of states in the conduction band increases rapidly as the temperature T goes well above $400\ K$. Thus, c-BN effectively becomes electrically conductive.

C-BN is of interest for high frequency and high-power applications, it has a relatively high dielectric permittivity constant (~ 7) [3] and high thermal conductivity (7.4 and 13W/(cm*K), experimental and theoretical value) in .Nguyen et al. fabricated a MIS- HFET (Metal Insulator Semiconductor Heterojunction Field Effect Transistor) prototype using BN as the insulator on an AlGaN/GaN structure, and a sapphire (Al_2O_3) substrate. The BN layer is deposited via RF Magnetron Sputtering from a hexagonal BN target at a working pressure of 0.21 Pa (1.5 mT) in a N_2/Ar gas mixture of 1:1, at room temperature. XRD (X-Ray Diffraction) measurements performed do not show a peak for BN suggesting an amorphous deposition. XPS

(X-Ray Photoelectron Spectroscopy) finds the peaks for the cubic and hexagonal forms of BN (c-BN, and h-BN). The Electron Binding Energy of h-BN is of 190.6 eV, and for c-BN approximately 191.5 eV [4], [5]. The deposition consisted mainly of the cubic phase. The authors reported a gate leakage current in the $10^{-9}A$ range. Low gate control for forward voltage suggest a strong mid-gap states interaction might be present at the BN/AlGaN interface. The device shows poor performance at temperatures reaching 400 K with low saturation current per unit area

Some works focus heavily in solving the Schrödinger's wave equation, because it is necessary to find the allowed energy states for an electron in crystal, and other physical characteristics that give rise to semiconductor electronic devices characteristics and operation. With an increase in demand for faster and more reliable devices there is a need of a more accurate, physical description of materials characteristics to accurately predict a device's operation. Si based technology makes use of physical models to predict their behavior as this approach is widely accepted [7]. The use of comprehensive physical models for device operation is beneficial to predict operation and to make reliable designs. Vipin, et al. make use of a computational model to analyze the behavior of an AlGaN/GaN HEMT and make comparison of experimental and calculated values with matching results. The authors discuss the importance of carrier and lattice thermal effects on the HEMT Source to Drain current. In chapter 5, this work makes a comparison of the theoretical estimate of carrier mobility Vs. the actual measurement through a Hall effect in a BN thin film. The theoretical calculations agree within less than an order of magnitude with experiment.

The authors in [10] AlGaN/GaN grown by MOVPE (Metal Organic Vapor Phase Epitaxy) on 4in Si substrates for investigating the high temperature (500 C) HFETs performance characterization. It is reported that carrier mobility of the 2DEG (2-Dimensional

Electron Gas) decreases with a “power rule of the temperature”. The authors used a GaN buffer layer for insulation from the Si substrate. It was found that the increase in drain current is comparable to that of HFET grown on sapphire. This means that performance is not affected by the thermal properties of the Si substrate with the buffer layer.

Thin-Film transistors TFT’s used as chemical sensors make use of 2-D materials and Fermi-Level tuning, which in turn is detected as a change in drain current. This is the principal mechanism of chemical detection in these devices. 2-D sensing materials however, have the disadvantage of direct contact between the analyte and the working material. A passivation layer might be added to prevent surface degradation, but this might lower the performance and sensitivity of the sensor in question. [11] present a MoS_2 Heterostructure TFT with a hexagonal Boron Nitride Passivation layer. The BN layer shows an increase in device reliability without sacrificing device performance. This is done by avoiding direct exposure of the sensing device to very active reactants, since BN is known to be chemically stable and oxidation resistant, even at high temperatures. The authors report a carrier mobility of 30 – 50 $cm^2/V*s$ (note that these mobility values belong to MoS_2). The sensing action was done by measuring the change in R over R as $\frac{\Delta R}{R}$ when specific gases were let into contact with the TFTs sensing surface. The authors also reported that devices with no surface passivation showed degradation of Ids by 60% after 2 days under ambient conditions, while devices with h-BN passivated surface showed no sign of degradation after a week under normal ambient conditions.

BORON NITRIDE THERMODYNAMIC STABILITY

Initially, the synthesis of c-BN was done at high temperature and pressure. Existing pressure-temperature phase diagrams do not cover a wide range for these parameters, i.e. if one wants to make use of the phase stability curves for synthesis in an ultrahigh vacuum. Instead those are commonly found in the range of 10 GPa and 3000 C. RF magnetron sputtering systems work in a high/ultra-high vacuum and it is worth mentioning that these are non-reversible processes. The authors in [15] investigated the phase stability of BN thin films done by RF sputtering while varying the substrate temperature and bias (- Voltage), at a constant pressure and a mixture of Ar and N2 sputtering gases. The authors present a phase diagram indicating that higher temperatures are favorable for the formation of the c-BN phase while at a lower temperature the h-BN phase is more stable, as is expected. Also, a more negative bias is also favorable for c-BN crystallization, but it is noted that this control parameter needs be limited due to re-sputtering from ion bombardment. The Hypothesis is that the thermal motion added to the high energy ion bombardment meets the requirements to synthetize c-BN.

A hexagonal Boron Nitride thin-film grown by MOCVD on Si. The h-BN is not shown by XRD since it is difficult to observe due to the small size of the BN nuclei [16]. The authors point out to the bulk and π plasmons present in XPS surveys since it is a differential characteristic between c-BN and h-BN. It is mentioned that both phases show the bulk plasmon in the B(1s) and N(1s) surveys, but only the h-BN has the π plasmon around 9eV higher than N(1s) and B(1s) while c-BN does not. This is used to determine the h-BN in the deposited thin-film. The growth conditions are 3mTorr, 900 ℃, for 6Hrs. This work shows h-BN obtained by

MOCVD with parameters like the ones used in RF Sputtering that yields c-BN presented latter in this work.

The evolution of the deposited film by IBAD is shown by HRTEM in [17]. The film in the h-BN (sp2 hybridization) phase and it evolves through a r-BN (rhombohedral) into the c-BN (sp3 hybridization). The goal is to optimize the h-BN deposition by staying away from the cubic lattice formation. The followed [18] stress formation model where sp3 does not become a stable phase until it is in the range of 4-5 GPa. The authors use a threshold value of momentum transfer [19]. With the ion energy at 480 eV the sp3 phase is existent. To keep the h-BN phase, the ion energy must be maintained below a threshold value of 450 eV. A phase existence diagram (in analogy with the phase-stability PT curves) shows the different sp2 and sp3 existence with Ar/B flux ratio in the abscissa and N/B in the ordinate. An existence diagram with stress Vs. flux ratio is also displayed to provide that the sp3 nuclei appears after reaching a stress threshold value.

The partial pressure of the sputtering gases used during a PDV process plays an important role in the crystal growth, formation, and evolution. The effects of the mixture of Ar and N2 vary with the atmospheric composition. [20] makes a deposition of c-BN on Si with buffer layer of B4C. The thin film composition is seen to have sp3 hybridization.

CHAPTER IV

MAGNETRON SPUTTERING PROCESS AND BN THIN FILM DEPOSITION

[49] The Magnetron Sputtering System (MSS) uses a Physical Vapor Deposition (PVD) process to vaporize a target. Sputtering gasses are employed in the process, with a combination of inert and reactive gases. This process takes place in a vacuum chamber. Where under low pressure the gas species will randomly lose an electron, thus become effectively ionized. Figure 4.1 below shows an Ultra High Vacuum chamber and load lock chamber set up like the one used in this work to produce the depositions. The image was taken from AJA systems website. The machine used in the work is made by AJA systems. Figure 4.2 shows the MSS at UTRGV and Figure 4.3 the plasma sputtering of a hexagonal Boron Nitride Target in the AJA sputtering system. The plasma is conformed by ion and neutral species of an Ar and N_2 mixture.

Figure 4.1 - Ultra High Vacuum (Main) Chamber and Load Lock Chamber with Gate Valve and glass windows

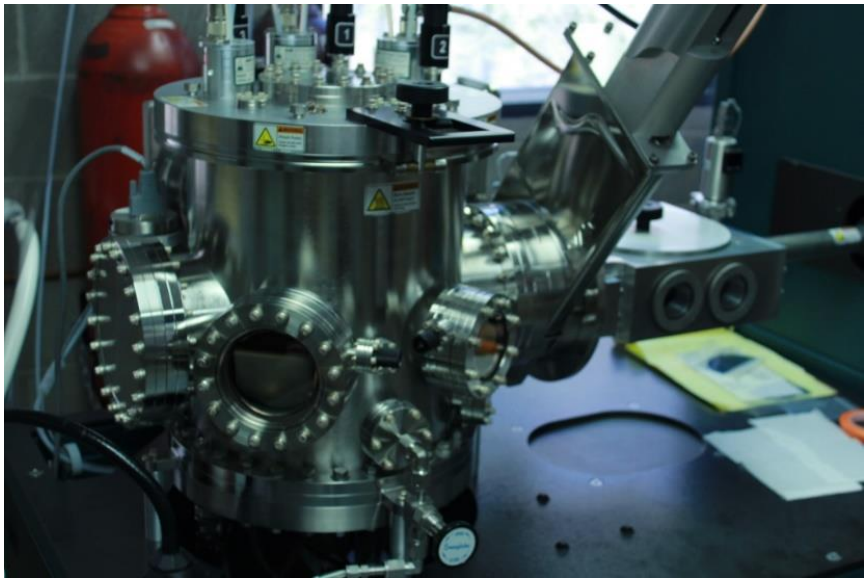

Figure 4.2 - The main chamber of the MSS at UTRGV

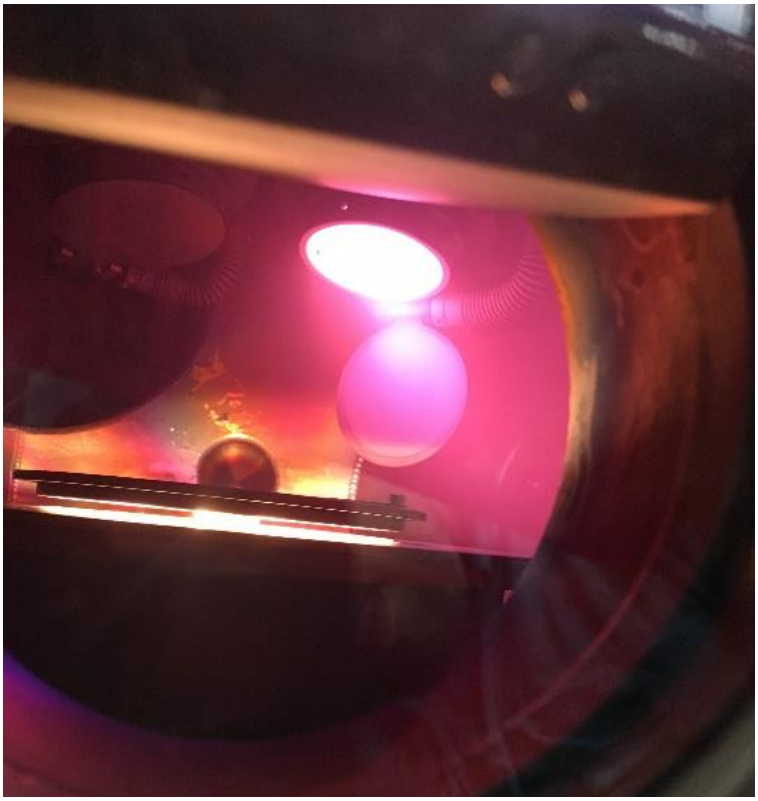

Figure 4.3 - RF Plasma Sputtering of h-BN target (MSS at UTRGV)

A negative bias voltage is applied to the target to accelerate the ionized species to the target's surface. The applied DC or RF fields turn the low-pressure gas into partially ionized plasma. If the ion speed is high enough, then the bonding energy of the target atoms is overcome, and a target atom will become sputtered. If the ion energy however, is too large, then ion implantation or target damage might occur. When sputtering occurs, the sputtered atoms travel at high speeds, and if they hit the substrate surface they might become deposited. The continuous deposition of sputtered atoms creates a thin film that can be a crystal or an amorphous formation. Such films are commonly utilized for metallization, electric or thermal contact, mechanical protection, and chemical passivation, among other uses. This is of importance for the

semiconductor and electronics industries because it allows for the growth of crystal structures of common and exotic materials, in the nanometer range, with a wide diameter of deposition ($\approx 4in$).

Selection of proper process variables is important. System parameters such as pressure and sputtering gas species are related to the minimum potential at which a plasma can be ignited. The variable process parameters include, the working pressure, and flow of sputtering gases, RF power, substrate temperature, and process time. The working pressure and the presence of sputtering gases at different ratios affect the process because this is related to the mean free path between collisions. As the pressure rises so does the energy requirement for electron-ion pair generation (the gas work function), and as the pressure gets lower, the mean-free path becomes greater and there isn't enough gas species in the vicinity to stabilize the ion-electron pair generation. Working pressures vary from 1mT to values greater than 60mT. An appropriate gas flow is necessary, the MSS significantly heats up the ionized gas particles, a continuous gas flow prevents the hot atom and ion build up, and therefore provides reliability to the deposition process.

Being able to control the temperature of the substrate by added thermal energy allows for sputtered species to diffuse through the substrate, new compounds to be formed, and allows for the nucleation on others that, otherwise, a desired phase formation might not get enough energy from its own momentum and the fast atom/ion bombardment to crystalize. The electric power parameters are directly related to the to how much energy is gained by the plasma, and it is released in the form of ion collisions to the surface of the target and other ions and neutrals in the chamber. These are the main mechanisms by which power dissipation occurs in the MSS.

When the MSS plasma is ignited, the individual plasma particles knock off the surface atoms of the target out of their place, if the sputtering gas particle has enough momentum, and exceeds the bonding energy of the surface atoms. The ejected target atom flies at high speeds (i.e. greater than the thermal velocity of the thermalized target atoms) and it deposits when it hits the surface of the substrate. Upon arrival, the deposited atom might form crystal structures with the substrate and other arriving atoms. If the thermal motion is high, the atom might diffuse deep into the substrate's surface. If the sputtering ions and neutrals are energetic enough, there is a possibility of re-sputter of the deposited atoms.

In this work the RF MSS is used to sputter and create functional thin films of group III-V compound semiconductor, these thin films are deposited in common semiconductor substrates such as Silicon (Si) and Sapphire (Al_2O_3). The Boron Nitride target is made up of the hexagonal crystal phase (h-BN). This h-BN has a white chalk like color and it is considered a soft material. Because of its wide bandgap h-BN is mostly seen as an electrical insulator, although it has potential for thermal transfer and chemical passivation. Figure 4.4 below shows a ceramic h-BN target provided by AJA systems for the MSS.

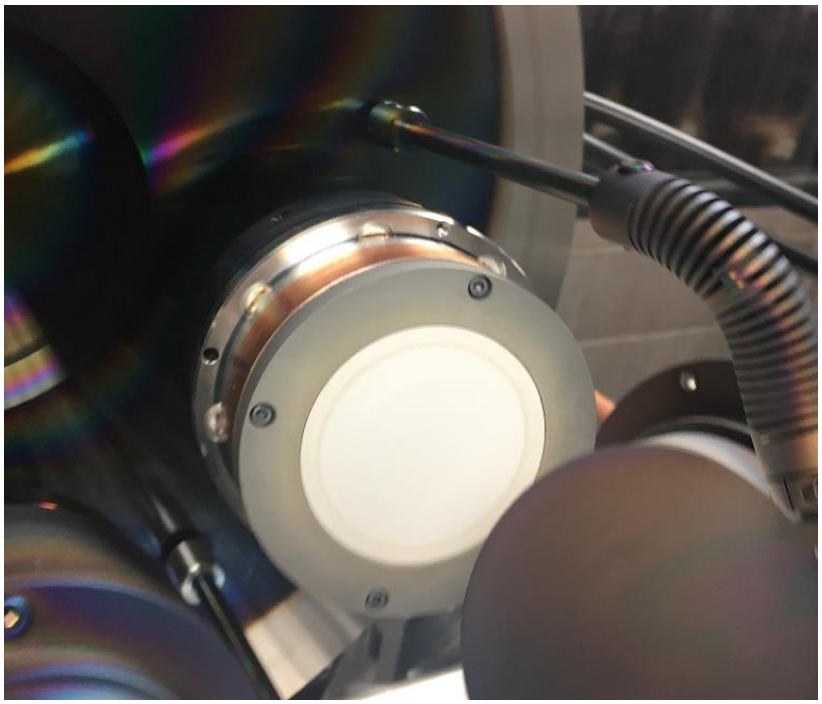

Figure 4.4 - h-BN target mounted in the RF gun of the MSS

For crystals to form, the right conditions need to be meet at the surface. This work does not go deep into the thermochemistry of crystallographic formation. One of the parameters that is commonly observed is lattice mismatch. Lattice mismatch is an issue because of accumulated stress requirements for different bond formations when a material is deposited on top of a material with a different lattice constant, there is normally what is called a nucleation layer, these layers serve as a transition until the desired material becomes synthetized.

In deposition tests performed with no thermal energy added to the Si substrate, no Boron, nor Nitrogen is detected by XPS elemental composition on the surface. Although a small temperature increment is observed due to ion and sputtered species bombardment, this is not enough to overcome the standard enthalpy of formation of either h-BN or c-BN. Experiments performed at 100℃ left the Si substrate with a blueish thin film, the film is opaque and soluble

in propylene (alcohol), indicating no crystallization. High quality III-V semiconductor have been grown over Si at high temperatures. Following these results, the temperature is set at a higher value for BN depositions. The crystalline thin-film is achieved with the substrate at 600℃, working pressure of 6mT, Ar to N2 sputtering gas flow ratio of 6sccm to 9sccm and 100 Watts of RF power to the target.

Depositions are made at this substrate temperature. Varying the deposition time, and the inert to reactive gas ratio. The films show a metallic blue to purple color, depending on the deposition time. These films are examined by XPS for elemental composition and chemical bond information. XRD was performed to identify the lattice structure, and SEM shows grain formation and size of the deposited crystals. Samples growth for 18Hrs and annealed at 800℃ show an ambar color just like the descriptions of the bulk material.

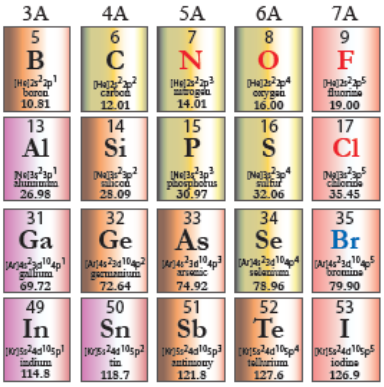

Figure 4.5 - Common materials used in semiconductor devices, from a downloadable periodic table available at http://periodic.lanl.gov/index.shtml

THE PLASMA ELECTRO-THERMODYNAMIC STATE OF THE SYSTEM

The Equation of State of an ideal gas is known to be

$$pV = nRT \tag{4.1}$$

where

$$n = \frac{m}{M} \tag{4.2}$$

This representation allows one to estimate either variable when the other 2 are known values, a more detailed discussion for the equation of state of gases can be found in any thermodynamics textbook. In the case of the MSS, the working pressure of the chamber is in $10^{-3}Torr$, in this work, the range might vary from 3mT to 30mT unless otherwise noted. Because the sputtering gases are stored separately, and the MSS is at a pressure difference with the storage units, for the rest of this work it will be assumed the gas either undergoes an isothermal transformation or it becomes thermalized very quickly upon entering the main chamber (where the sputtering and deposition takes place). If the system is made up of different gas species, then the total pressure is made up each species partial pressures [12][13][14].

The equation of state computes the number of atoms per unit volume, or density in the atmosphere, e.g. if the environment is composed 100% of Ar. In a volume V of $1cm^3$, at a temperature T of $300K$, and pressure p of $6mT$. The equation of state

$$pV = \frac{m}{M}RT = nRT \tag{4.3}$$

$$6mTorr \times \left(\frac{133.322Pa}{Torr}\right) \times 1cm^3 \times \left(\frac{10^{-6}m^3}{cm^3}\right) = n \times \left(8.314\frac{J}{K \times mol}\right) \times 300K \tag{4.4}$$

The equation of state is used to compute values for the density of gas particles in a system. The equation yields the following values for the density of Ar gas at a pressure of 6mT.

$$n = 3.206 \times 10^{-10} moles/cm^3 \tag{4.5}$$

$$\rho = 1.931 \times 10^{14} cm^{-3} \tag{4.6}$$

$$M_{Ar} = 39.95 g/mol \tag{4.7}$$

$$d = 1.28 \times 10^{-8} g/cm^3 \tag{4.8}$$

At very low pressures, gas species become randomly ionized by atom-atom impact or by stray electrons (atom species become effectively charged). The working pressures inside RF Magnetron Sputtering System fall in this range. Ionization occurs because although the gas collisions are assumed to be elastic, there is a probability of net momentum transfer between collision. This occurs because the velocity distribution in a gas, at thermal equilibrium is given by the Maxwell-Boltzmann velocity distribution function $f(T)$.

Any plasma would eventually die out without a supply of energy to sustain the RF emissions and oscillations. Sustained plasma oscillations are possible due to the RF supply through the sputtering target. The ion-electron pair generation rate is outside of the scope of this work.

There are two things to note that are of the outmost importance to make sure we do not get confused about the physical processes going on in the MSS. The first is that ionization of the gas species does not constitute a plasma. The word plasma is commonly used to describe the averaged macroscopic properties of the microscopic phenomena that are characteristic of plasmas (e.g. the ion-electron density and frequency of oscillation). The second is that the PVD process that goes on inside the MSS is a non-reversible process and that through the sputtering,

the system is not under thermodynamic equilibrium. Nonetheless, because the temperature and differential pressure of the system are kept constant we can treat the process as if it was under equilibrium and the irreversibility of the process is implied when we talk about the heat of formation and different thermochemical phases of Boron Nitride.

PLASMA THEORY AND MAGNETRON SPUTTERING ION SPECIES

Because the power dissipated by the system is a known process parameter, it is instinctive to attempt to model the electrothermal transfer by using the target as a linear resistance. For ceramic targets the resistance approach fails, especially for ceramic target with high resistivity. As a result, it should be obvious as to why ceramic targets make use of RF power for sputtering rather than DC [41].

The h-BN phase has a known resistivity of $10^4 \Omega/cm$. An applied power of 100 Watts at, 17 Volts means that the supplied electric current of I = 5.882 Amps does not go through the highly resistive target (note that this approach could be considered if one were doing DC sputtering, ergo a conductive metal target). The h-BN target impedance is given by equation (9)

$$Z = \rho \frac{d}{A} = 10^4 \frac{0.005}{\pi \times 0.0254^2} = 24.6\ K\Omega \tag{4.9}$$

Where the resistivity of the h-BN target is $10^4\ \Omega cm^{-1}$.

The target would dissipate over $850\ KW$ for the given current I. This shows that the energy is being transferred to the electrically charged plasma via the RF fields and not through electric conduction trough the target.

The stable plasma however is highly conductive due to the relatively high ion-electron pair density. Because of this, the magnetron sputter uses the AC source to sputter ceramic targets that transfer power by using a capacitive approach, where the Radio Frequency (RF) fields reach through the dielectric material (the ceramic target).

HOT ION PARTICLES

The ionized species get accelerated through an electromagnetic field, due to the Lorentz Force. The complete electrodynamic expression of the force felt by a charged particle moving in an electromagnetic potential is given by

$$\boldsymbol{F} = q(\boldsymbol{E} + \boldsymbol{v} \times \boldsymbol{B}) \tag{4.10}$$

The effect of the Electric Field on the ion species is to accelerate them to the target for sputtering, while the magnetic field has no net contribution to the kinetic energy. The Magnetic Field acts on the normal component of velocity of the ion species and focuses the collisions on the target surface. For simplicity, here the focus is to describe the effects of the Coulomb force on the ion species rather than to use the complete Lorenz description.

$$\boldsymbol{F} = q\boldsymbol{E} \tag{4.11}$$

Among the effects commonly observed in plasma discharges are the RF emissions and the corresponding Debye length arising from ion-electron oscillation and ion-electron pair density, and optical emissions. Plasmas can become anisotropic under certain geometry of the applied fields, but the analysis of the anisotropic effects is beyond the scope of this work, here we consider isotropic plasmas that model the sputter deposition chamber. If there are enough collisions in the fully or partially ionized plasma, and the system is at thermal equilibrium, then a

Maxwellian distribution is a good representation of the system. The number density of the individual ion species, n_s $[cm^{-3}]$, and the Debye length, are basic characteristics of the system. The Debye length, λ_D $[m]$, is the displacement of an accumulation of charged ions and electrons that oscillate according to Hook's law for harmonic oscillators. This oscillation causes RF emission.

From kinetic theory, and because the velocity distribution is Maxwellian, the most probable speed for a species is given by equation (12), and the average kinetic energy by equation (13) as

$$v_{th} = \sqrt{\frac{8kT_s}{\pi m_s}} \tag{4.12}$$

$$E_k = \frac{1}{2} m_s {v_{th}}^2 = \frac{8kT_s}{2\pi} \tag{4.13}$$

Where v_{th} motion (thermal velocity) is the most probable speed due to thermal motion. It should be obvious that the variable relating the average velocity to the state of the system is the thermodynamic temperature of the system. it is for this reason that in subsequent chapters we consider the state of the system in order to investigate the processes that take place during sputtering. For Ar at a temperature of 298.1 K [25℃] v_{th} is $397.287 m/s$. For a 1 particle system, the total energy is given by

$$W = E_k + \Phi(\mathrm{r}, \mathrm{t}) \tag{4.14}$$

The second term in the right-hand side of the equation is due to the potential felt by the particle. In this work, the discussion is restricted to the potential due to the electric field from the

applied RF input to the system. In the MSS, the average ion reaches velocities in the range of $10^4 m/s$, and these high velocities are directly related to the applied electric power.

To model the complete circuit a cylindrical approximation to model the ongoing process in the main chamber is used. As a first approximation, it is common to represent the plasma as a linear resistance. Plasma theory developed from magnetohydrodynamic and the kinetic theory of gases provides the formulation to calculate the number density of the ionized species based in this linear resistance model and it is Ohms Law. This result is agreement with known values of plasma density found by researchers ($\sim 10^{10} cm^{-3}$) that make use of the Langmuir probe approach for measurement of the Debye length λ_D. With knowledge of the plasma parameters the sputtering process can be further analyzed. The rate of collision and average speed of the impingement ions are known. Instead of using classical mechanics to compute the momentum transfer in a collision between fast ion and a semi-stationary target atom, this approach is to average the energy of the partially ionized plasma and is used to compute the sputtering rate from the thermal conduction stand point and the standard enthalpy of formation of the sputtered species, with knowledge that the target atoms are bombarded by the high speed ions from the partially ionized plasma.

We start with the assumption that the gas is at a uniform temperature, and when at low pressure a gas atom becomes ionized it is at the same temperature as the its environment, and thus the thermal velocity is the same (although this assumption is idealistic), this assumption is useful because the partially ionized plasma used in the RF MSS is in a *steady state*. The ion species gains velocity when accelerated through an electric potential, i.e. the applied RF electric field at the target. In general, plasmas can be treated as being quasi-neutral, since most charge separation is immediately compensated by the respective coulomb force and keeps the system at

equilibrium, this causes an oscillation that is of the form of hooks law. This quasi-neutrality implies that there are no long-range electric fields present. Then again, this assumption can only be made in the macroscopic scale. It is useful to get full picture and realize that electron sheets tend to form in the surrounding of ungrounded surfaces, and that the macroscopic approximation falls apart when the scale is comparable to the Debye length. Also, although there are no long-range electrostatic fields, there may be an RF emission during arc discharges. Figure 4.6 shows an arc discharge on a high voltage line in a test facility in Siberia.

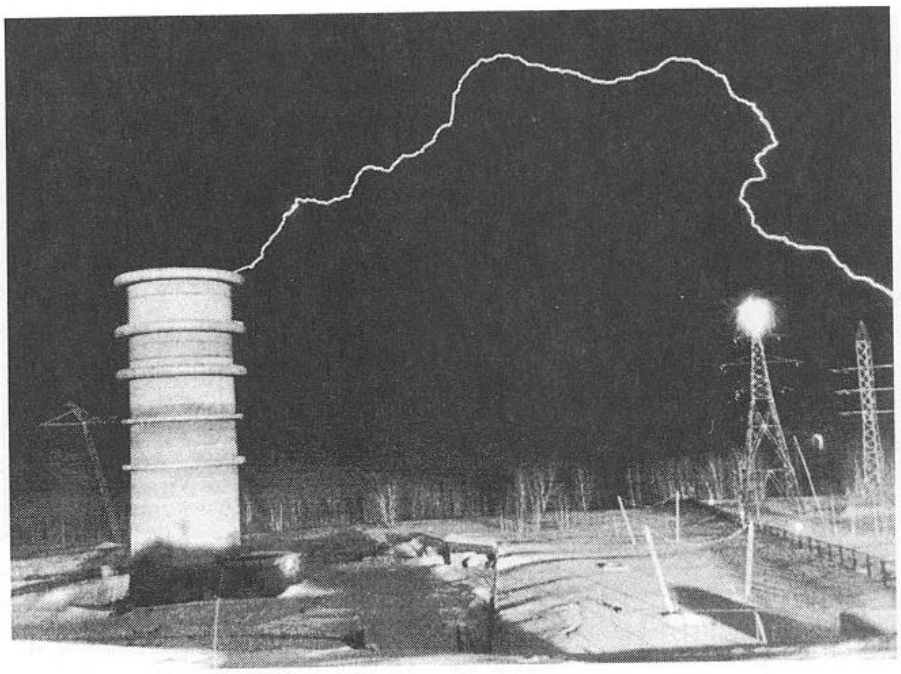

Figure 4.6 - Arc Discharge on a 110 KV Transmission Line, http://www.capturedlightning.com/frames/longarc.htm

Early plasma research showed that when a probe is introduced to the plasma, the probe acquires a negative surface charge sheet. This seems counter intuitive since the target is biased

with a negative voltage. This occurs because electrons have much greater thermal speed than ions, and tend to immediately populate ungrounded surfaces, producing a surface potential with the ions.

At the target surface, these electrons will feel a repulsive electric potential from the source and attraction to the shielding ions accumulated across. The total resulting electric field is the linear-spatial addition of the target-source field and the accumulated charges. Because of the shielding effect, only ions close to the surface charge sheet are in the presence of the resulting attracting potential to the target, and thus only the ions in the charge region have a high probability of accelerating towards the target and effectively sputtering a target atom. The total kinetic energy of the ion upon collision with the target is given by

$$E_{coll} = \frac{1}{2} m_s {v_{th}}^2 + \phi(x) \tag{4.15}$$

where m_s is the mass of the species, v_{th} is the thermal speed at 298.1 K, $\phi(x)$ is the potential felt by the ion at a distance x, from the target. Although a macroscopic thermal transfer approach will be introduced it is good for intuition to mention the general idea of kinetic sputtering. The binding energy of the target atoms is E_{target}. If $E_{coll} > E_{target}$, then sputtering is highly probable, and the atoms is ejected in a random direction with a net speed gain obtained from the difference in the collisional and binding energy and net momentum transfer.

When a sputtering gas particle becomes randomly ionized inside the MSS it gets accelerated toward the target by the action of the RF electric field. The sputtering ion collision speed with the target can be calculated by the classical approximation of motion.

$$U = Kinetic + Potential \tag{4.16}$$

$$U = \frac{1}{2}mv^2 + xF \tag{4.17}$$

where U is the total energy of the particle, K and P are the kinetic and potential components, respectively. F is the potential field and x is the distance from the substrate, to the target, and v is taken to eb the initial speed of the particle, or the thermal speed (i.e. given there isn't any thermal build up in the ionized and neutral gas species). With the electric field E is equated to the coulombic force felt by the ion particle.

As already mentioned of following a complete kinematic approach, this work makes use of electrodynamics to compute the energy gain by an individual ionized plasma particle. It then moves to include the thermal effects on the system, assuming the system is thermalized. This in part is due to the plasma not considered to be fully ionized, and the continuous pumping of the vacuum system prevents the plasma from becoming a hot-full ionized plasma. The following schematic represents the model of the plasma sputtering chamber with the negative bias at the target.

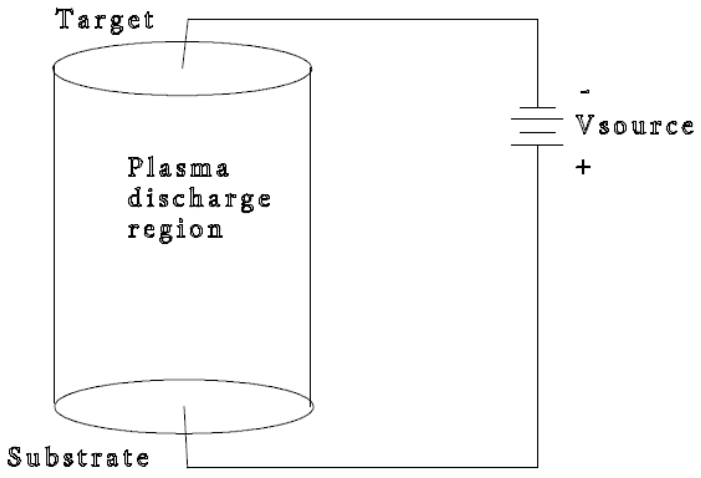

Figure 4.7 - Plasma discharge region, cylindrical approximation model

The plasma is modeled as a uniform piece of conductor and thus the electric field is given by the ratio of the voltage to the distance from the target to the substrate. From this, the Coulomb potential is also derived.

$$E = V/r \tag{4.18}$$

$$F = qE = q\frac{V}{r} \tag{4.19}$$

The substrate to target distance is approximately 20cm. Because inside the plasma, the potential is assumed to be constant, as given by the cylindrical model. This gives us the acceleration by including the particle mass and Newtonian mechanics and equating the Coulombic force to the classical term. Note that the symbols for acceleration, a, and $\ddot{x}$, might be used interchangeably.

$$F = qE = m\ddot{x} \tag{4.20}$$

$$\ddot{x} = qE/m \tag{4.21}$$

Then the equations of motion are solved to yield the collisional speed of ionized plasma gas species. Because the plasma is partially ionized, and the neutral to ion ratio is significant, Dalton's law of molar fractions is useful to derive an expression of the equivalent temperature of the system. Dalton's law is used assuming we can think of the gases in the plasma as ideal gases, this is the basis of using the RF electrothermal transfer approximation in this approach. These expressions are implemented in the thermal ion sputter rate developed here.

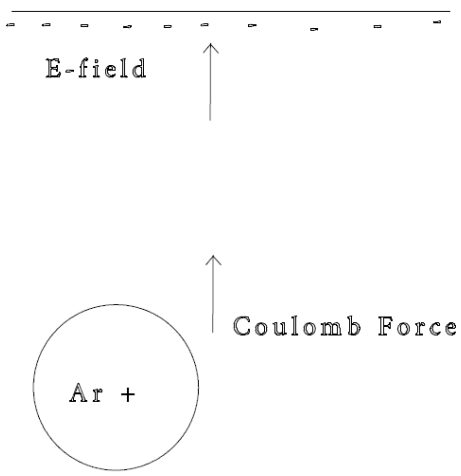

Figure 4.8 - ionized Ar species in accelerated in a field force

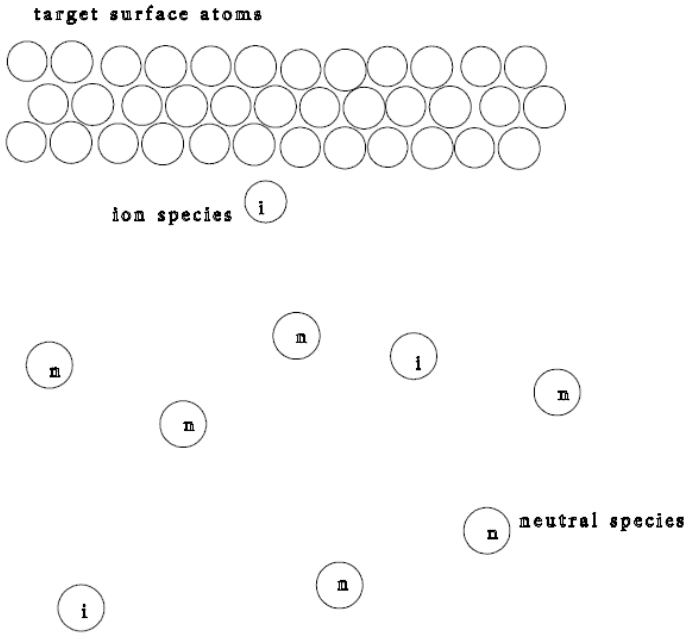

Figure 4.9 - Neutral-ion species near the target surface

$$\dot{x}_f = \dot{x}_0 + \ddot{x}t \tag{4.22}$$

$$x = x_0 + \dot{x}t + \frac{1}{2}\ddot{x}t^2 \tag{4.23}$$

Because the cylindrical approximation for the plasma model as an electric circuit assumes uniform conductivity throughout the plasma, the electric field inside is that inside of a uniform conductor, and thus takes the form of the Poison distribution for the E field, as previously shown. For the ionized species, this means that the ion accelerates through a constant potential field.

For the source voltage we use the rms values, and assuming the RF system is matched it has a VSWR that's very close to 1. At the operating frequency of 13.8 MHz, the wavelength of the EM wave is 21.739 meters. The wavelength is greater than our plasma model in length (20cm approximately) by 2 orders of magnitude and phase variation is ignored. We can then treat the system as having a uniform electric field throughout the plasma and use rms values to continue our computations. Known operational values for the voltage of the system are plugged into the equations described above.

$$E = \frac{V}{r} = \frac{17V}{20cm} = 85\frac{V}{m} \tag{4.24}$$

This yields an acceleration of $2.052x10^8\ m/s^2$. And with the initial particle speed being equal to the thermal speed we have initial velocities of $397.31\ m/s$ for an Ar ion. The thermal speed values can be looked up online or calculated from the known equation for average velocity of gases and thermal speed of molecules.

In the case where neutral becomes randomly ionized close to the substrate (i.e. far away from the target or RF source), it has the longest path to target collision, and thus, the longer it can accelerate. This implies that this is the maximum kinetic energy the ion particle can achieve in the plasma. In calculating the ion species speeds from electrodynamics and classical mechanics,

it is necessary to solve the quadratic equation of motion for the time variable. The resulting solution is of the form

$$t = \left[-(-2Vth) \pm \sqrt{4Vth^2 - 16\alpha x}\right]/2 \quad (4.25)$$

Where Vth is the thermal velocity described in the preceding paragraphs, α is the acceleration, and x (x must be replaced by x/π in the expression above) is the mean free path of the Ar gas at the working pressure and temperature parameters equals 3.5cm/π. The equation above yields a maximum flight time between ionization and collision of $9.37\ us$. The maximum time between ion-target collision happens between 129 periods of the 13.8MHz source. Achieving a collisional velocity of $2{,}321\ m/s$. This is equivalent to 1.115 eV for Ar. The classical kinetic energy and thermal velocity expressions are used to compute the actual temperature of the ion species.

$$T = \frac{2\pi E}{8k} = 10{,}163.86\ K \quad (4.26)$$

Where k is the Boltzmann constant and it is equal to $8.616 \times 10^{-5} eV/K$, and K is the unit of temperature in degrees Kelvin. And E is the classical kinetic energy of the particle in electron Volts. Note the individual ion temperature is raised to 10,000 degrees Kelvin. In comparison, an acetylene torch reaches values above 3,000 K, an industrial plasma cutter can go as high as 20,000 K, the surface of the sun is estimated to be 5,778 K, and the ITER Tokamak must reach $150 \times 10^6\ K$ for the plasma process to occur.

The ion density in sputtering plasma systems can be measured by means of a Langmuir probe. The ion species density is known to be close to $10^{-10} mol * cm^{-3}$, for similar plasma conditions to the ones used in this work (~6mT, 100Watts). The neutral species density is computed from the equation of the law of perfect gases. The purpose of this is to make use of

Dalton's law and the idea of molar fractions to calculate the equivalent temperature of the plasma system and make use of the ideas of thermochemistry and heat transfer to model the plasma sputtering system with the variables previously described. This results in a thermal model for estimating the target sputtering rate.

From the ideal gas equation, we find n for Ar to be $3.3x10^{-10}$mol per cubic cm, at 3mT pressure and standard temperature of 298.1 K. We rewrite he law of perfect gas to include both the neutral and the ion species. The cm is used as the basic unit of length for some of these calculations, but care must be taken since the electrodynamic calculations previously done were done in the meter scale.

$$pV = (n_1T_1 + n_2T_2)R \tag{4.27}$$

$$nT = n_1T_1 + n_2T_2 \tag{2.28}$$

With known values of the ion density of $1 \times 10^{10} cm^{-3}$, we can compute the total energy content of the system per cubic centimeter and the new equivalent temperature as

$$U = 1.47 \times 10^{-6}\, J * cm^{-3}$$

$$T' = \frac{U}{nR} = 328.899\, K \tag{4.29}$$

Where $n = n1 + n2 \approx n1$ for $n1 \gg n2$.

The Law of heat transfer in combination with an estimate of the probability that the ion accelerating from the longest distance (the substrate) will result in collision with the target and produce sputtering from the target atoms.

$$H = -kA\frac{\Delta T}{\Delta x} = -4.148 \times 10^{-3} * \Delta T \tag{4.30}$$

$$\Delta T = T' - T = 30.799 \tag{4.31}$$

And Δx is the distance through the thermal contact.

A modification of the law of heat transfer is made, to consider the lower pressure and the fact that not all the ions in the plasma accelerate through the full length of the distance between the substrate and the target. This is instead taken as a maximum distance that yields a maximum for the kinetic energy of the sputtering species.

$$f = f(\sigma, x) = \sigma/x \tag{4.32}$$

$$H' = Hf \tag{4.33}$$

In the above equation, f, is a function of the mean free path σ of the particle in a gas with thermal speed v_{th}, and x is the distance from the substrate to target (this region constitutes the space sample for the plasma model used here). The erosion rate or sputter is given by the ratio of the heat transfer to the standard enthalpy of formation ΔH_f°, of the target material. The sputter S is given by equation (4.34)

$$S = \frac{Hf}{\Delta H_f^\circ} = \frac{-kA}{\Delta H_f^\circ} * \frac{\Delta T}{\Delta x} * \sigma/x \tag{4.34}$$

The result of sputter equation is compared to experiment by measuring the difference in mass in the ceramic target, as is our case. There will be deviations from this, as we expect the redeposition of BN on the h-BN target, visual inspection of the target shows a growth ring in the outside of the target. This is due to the redeposition effect. The reason why this ring is only visible in the outside diameter of the target is because most of the sputtering occurs towards the middle due to the focusing effect from the magnetic field from the permanent magnet arrangement on the back of the target plate, while redeposition can have a wider outer diameter.

Mass difference measurement in the from the target indicate an erosion rate of 10.5mg/hr. the calculation performed above yield values of 16mg/hr. The difference is taken to account for redeposition. The redeposition phenomenon is not examined in this work. The process is 10.5/16 within the actual value.

The deposited Thin-Film

The atoms at the surface of the target are ejected at high speeds from the sputtering. The high-speed atoms collide with the substrate. There is a chance that the sputtered atom will become deposited in the new surface. The matter that arrives at the substrate will crystalize if there's enough energy available from the sputtered atom and backscattered ions and neutral gases that collide with the substrate. Adding thermal energy to the system by heating up the substrate is helpful for process control and one can achieve different thermodynamic phases that might not be possible while running the process without added thermal energy. The newly deposited atoms will form the thin film form the basis for testing the properties of the newly formed materials.

Figures (4.10) and (4.11) show thin films of Copper and Boron Nitride respectively. The Cu thin film was grown over a microscope slide (glass) without added thermal energy for 1 Hr. The BN thin film was grown over Si substrate at the previously mentioned 600 ℃ for 9 Hrs.

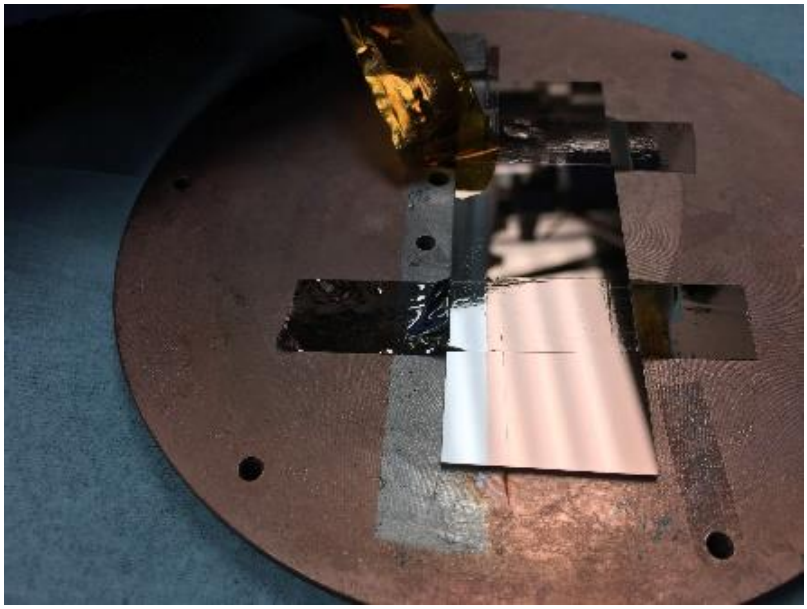

Figure 4.10 - Copper deposition/metalization on microscope slide (glass)

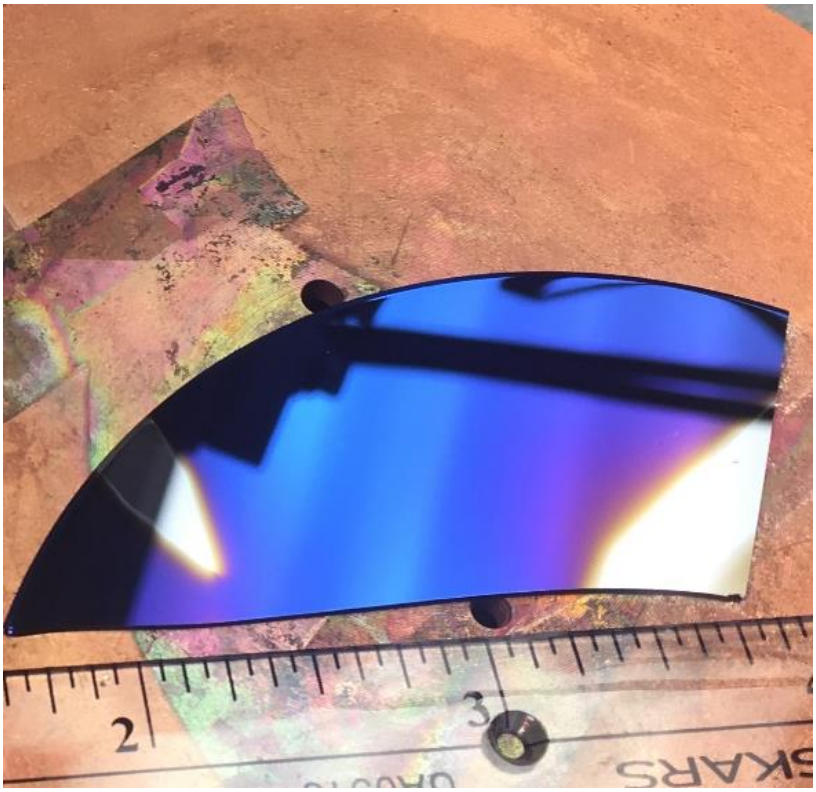

Figure 4.11 - BN thin film grown in Si substrate

CHAPTER V

THE CUBIC BORON NITRIDE THIN FILM

A WIDE BAND-GAP SEMICONDUCTOR

Cubic Boron Nitride has an indirect energy bandgap E_g of 6.1 eV approximately. For this reason, it falls into the category of wide band-gap (WBG) [5]. The wide bandgap semiconductors are sometimes used as insulators. It is because of this wide band-gap that there exists a low probability for the charge carrier to occupy the conduction band, i.e. for the given atom to become ionized. The probability of occupancy of the conduction band is given by the Fermi-Dirac distribution $f(E)$, and it is usually substituted by the Boltzmann approximation. The Fermi distribution is a function of the chemical potential, it tends towards the middle of the energy gap at room temperature. Ergo the c-BN thin film is expected to behave as an electric insulator.

Because the high energy required for a charge carrier to move to the conduction band, charge carriers that contribute to conduction have a much greater velocity in wide band-gap materials than in more conventional semiconductors. These make WBG materials good candidates for high power applications. However, this work only tests the c-BN thin films at room temperature and low electric fields.

THE BN GROWN ON SI 100

The Thin film depositions are done at various process times and with a combination of inert and reactive sputtering gasses. This is the process described in the previous chapter, in which the electrically excited plasma species sputter the target material. The target material atoms are ejected at high speeds and become deposited in the substrate surface, thus creating a thin film [15].

Results are observed as follows. The c-BN thin films grown by RF Magnetron sputtering were investigated for their chemical composition and crystal structure. Chemical stoichiometry is verified via X-Ray Photoelectron Spectroscopy (XPS). Crystal structure is confirmed via XPS and X-Ray Diffraction (XRD). Grain formation and grain size is seen through Atom Force Microscopy (AFM) and Scanning Electron Microscopy (SEM). The thickness measurement of the thin film is returned by the XPS and an average rate of deposition of 50nm/Hr is obtained.

Scanning Electron Microscope and Atom Force Microscope

AFM and SEM show grain formation and provide information on grain size. The grain size formation varies, depending on the sputtering gas ratio. This is due to the residual energy from backscattered high energy ions and neutrals after impact with the target. These ions or neutrals have different kinetic energy, as seen from the kinetic theory of gases. In this way, an Ar neutral at thermodynamic temperature T, has a different speed than an N_2 neutral at the same temperature. This is due to the difference in the molecule's nuclear mass, and that N_2 is a diatomic molecule while Ar is monoatomic. The energy of the backscattered species adds to the thermo-chemical processes and phase transformation [43][44][45][46].

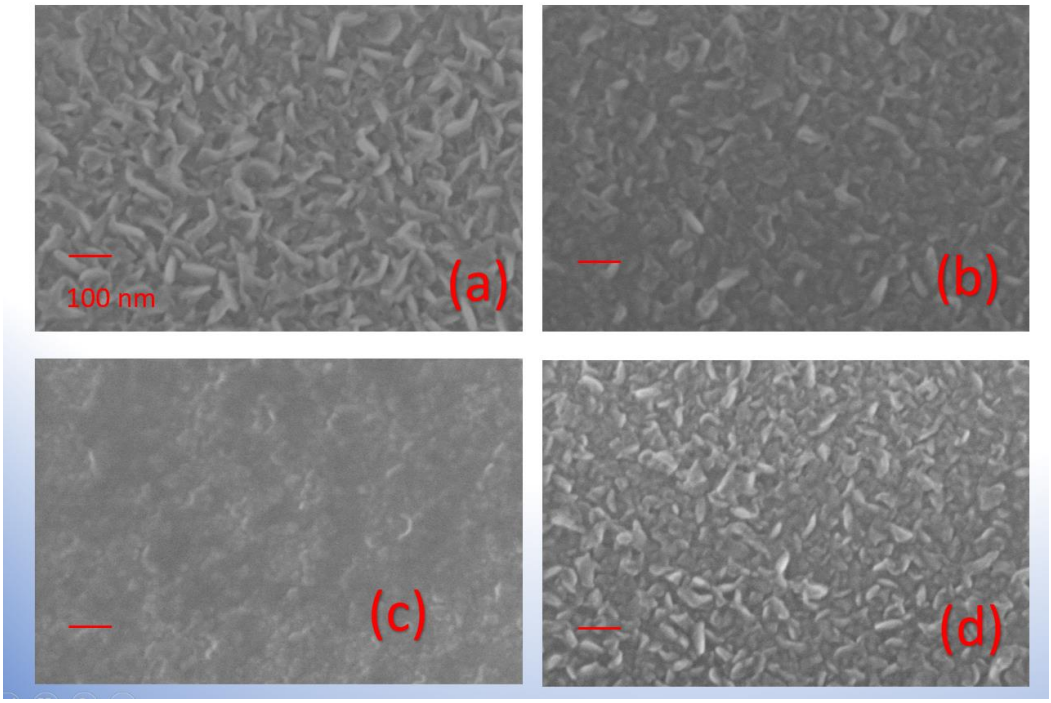

Figure 5.1 - SEM imaging of BN thin film grains grown on Si 100

Table 5.1 – Gas Flow ratio for processes in Figure 5.1

Ar/N_2 flow ratio (sccm) for the 9 Hr. Processes in figure 5.1	
5.1 (a)	0/9
5.1 (b)	3/9
5.1 (c)	6/9
5.1 (d)	9/9

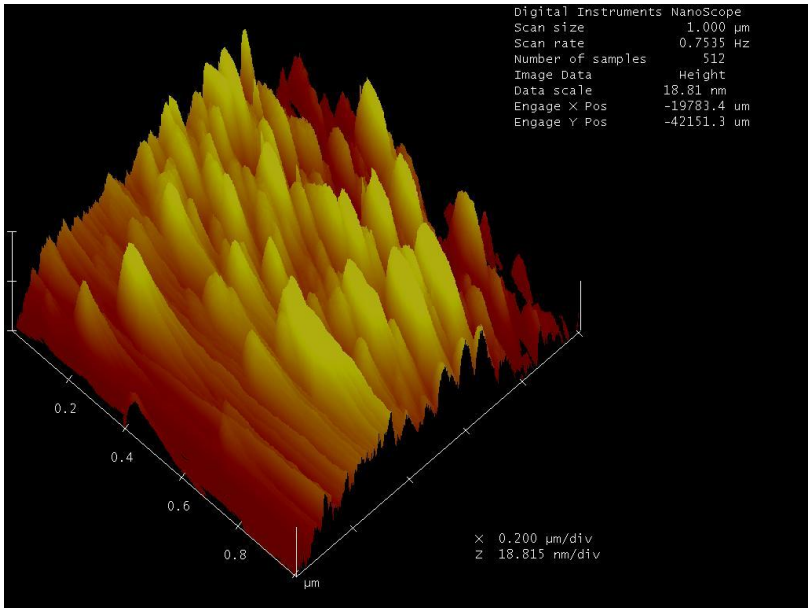

Figure 5.2 - Atom Force Microscope imaging of BN thin film on Si

X-Ray Photoelectron Spectroscopy

X-Ray Photoelectron Spectroscopy is used to analyze the chemical composition of the physical vapor deposited thin films. The XPS [40][42] surface surveys return the core electron binding energy of the atom species in sample. It also provides information on the thickness of the samples. Values for the core electron binding energy of different species are known, plus known difference in the spectra generated from different thermodynamic material phases. The National Institute of Standards and Technology (NIST) provides a list for many polymers and compounds, one may use the surveys provided to identify the crystal or polymer that is being worked [47].

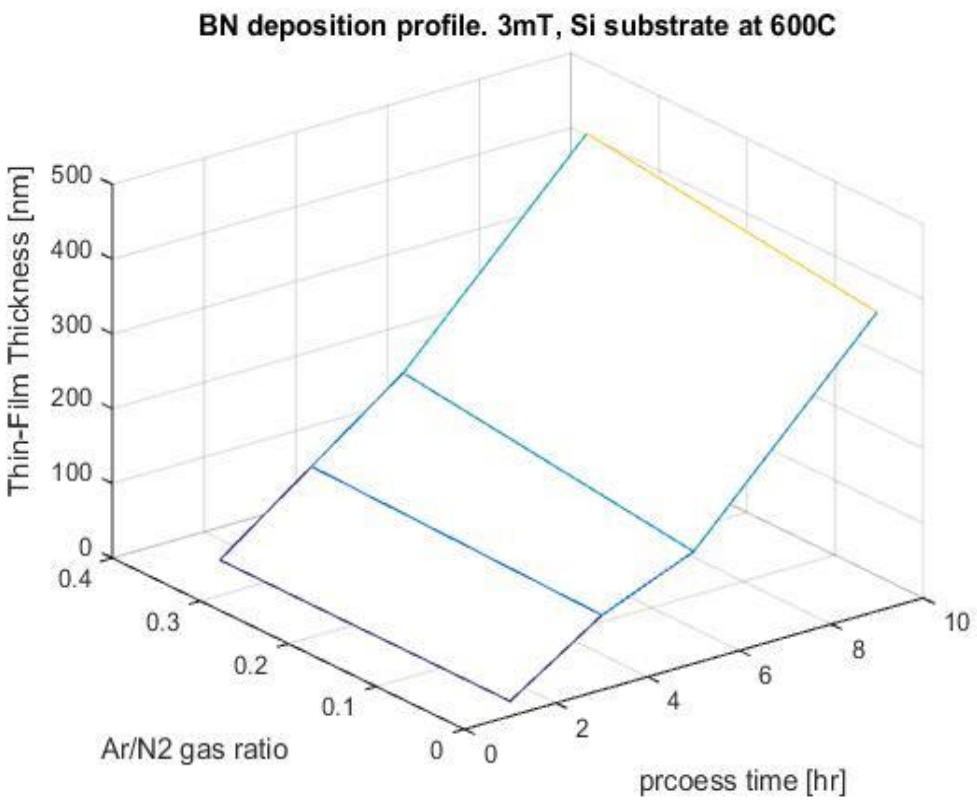

Figure 5.3 - BN thin film deposition rate, obtained by XPS

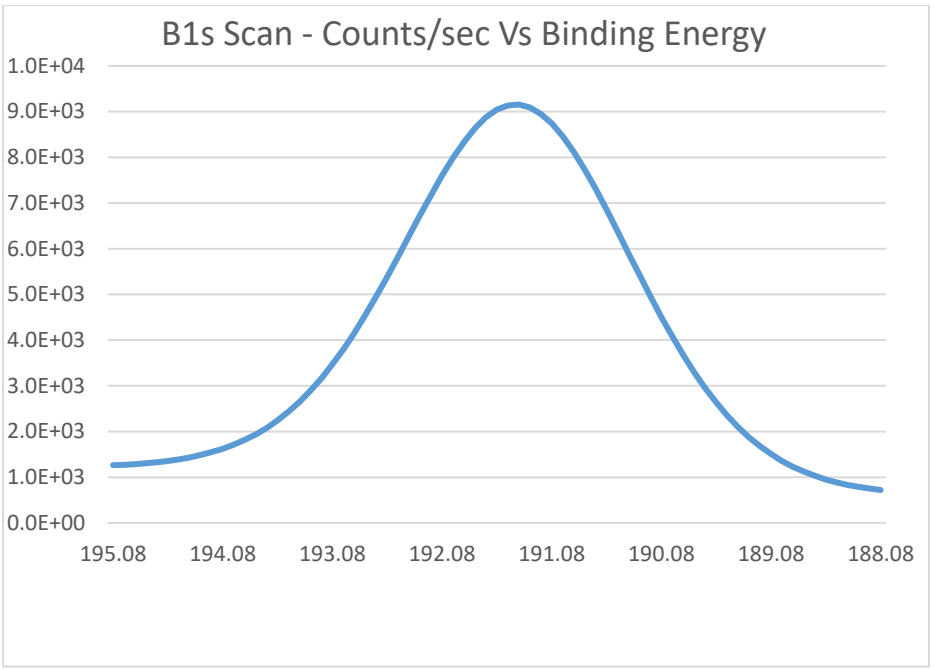

Figure 5.4 - B1s core electron binding energy by XPS

[26][27] The core electron binding energy of elemental Boron, S1, is of 189 eV. The Boron atoms in the wurtzite form of BN, or h-BN (for hexagonal) is found to be in the range of 190 eV. The Boron in zinc-blend, or cubic form of BN, c-BN is found to have a core electron binding energy of 191 eV. The XPS surveys suggest that the RF Magnetron Sputtering deposited BN thin films consist mostly of the zinc-blend phase of BN [32][33][34], at the current thermodynamic process conditions. The X-Ray Photoelectron Spectroscope also gives information on the thickness of the fabricated samples with a deposition rate of 50nm/hr. X-Ray Diffraction (XRD) is commonly used to identify crystal structures in solids and crystal size. XRD identified the surface as the cubic phase of BN.

It is concluded by the results obtained from XPS and XRD that the deposited thin films consist mostly of the c-BN phase. The Boron Nitride compounds are analogous to carbon. The

wurtzite form has the same crystal structure as graphite, and both are considered soft materials, although unlike graphite, h-BN is an electrical insulator. The cubic phase of BN is analogous to the cubic phase of carbon (diamond) [8][9][10][11]. Like diamond, c-BN is considered a super hard material [13] and it is second to this one in this respect. The cubic phase is found to be inherently p-type and can be doped with either donor or acceptor impurities [21][22][23][24].

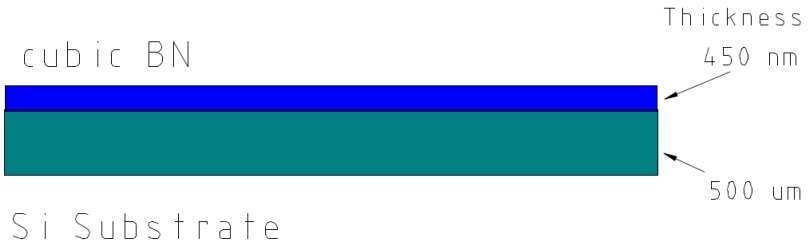

Figure 5.5 - c-BN thin film on Si traverse representation

ELECTRIC PROPERTIES OF CUBIC BORON NITRIDE

The electrical characteristics such as charge carrier mobility, and charge carrier concentration of these thin films can be evaluated by a theoretical calculation and Hall Effect measurement.

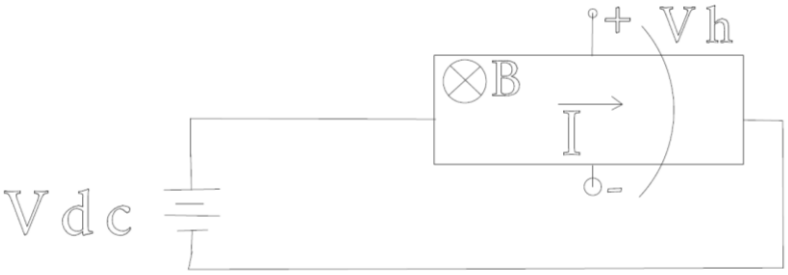

Figure 5.6 - Hall Voltage Measurement Schematic

For an estimation of the hole, or positive charge carrier mobility, knowledge of the physical characteristics of the semiconductor [16][17][18][19][28] are needed such impurity concentration, lattice constant, and grain size. The hole has a known mas of $m_p = 1.672 \times 10^{-27} Kg$, and the thermal velocity is $2{,}511.5 m/s$. The known grain size for a given sample is of 5nm for the most uniformly achieved thin film (figure 5.1-c). The average time between collision is approximated by the ratio of the grain size to the carrier speed. By definition, equation (5.1) [36][37][38][39]

$$u \equiv qt/m. \tag{5.1}$$

This yields for hole mobility

$$\mu_p = 1.906 \times 10^{-2} cm^2 V^{-1} s^{-1}.$$

The Hall Voltage Measurement is done following the guide provided by the National Institute of Standards and Technology (NIST). An out of the shelf permanent magnet is used as the source of the magnetic field needed to produce a deflection in the moving electric charges. Use is made of a Texas Instruments DRV5053 Analog-Bipolar Hall Effect Sensor to measure the Magnetic Field Density $\vec{B}$. The Hall sensor has a sensitivity of -11mV/m, with a saturation field of 73mT. The magnet measured values of $\vec{B} = 900\ Gauss$ with the sensor next to either the South pole or North pole face of the magnet.

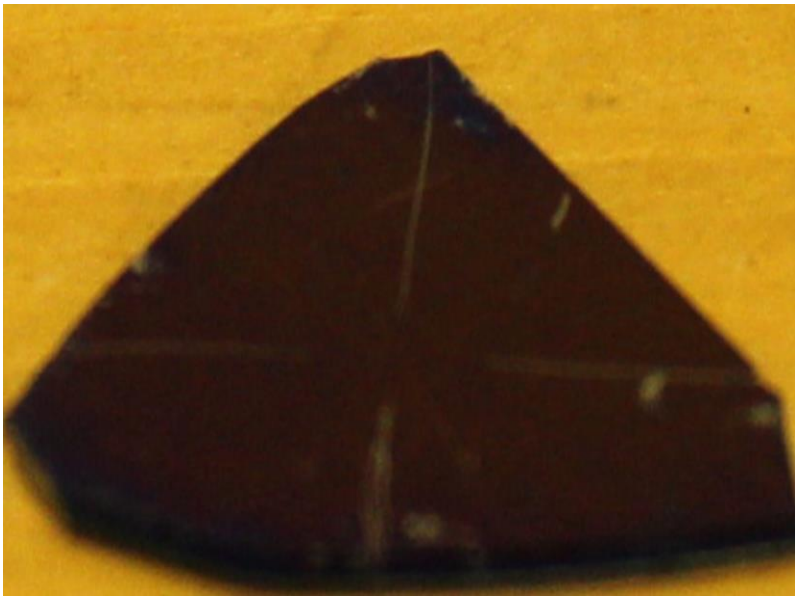

Figure 5.7 - cBN thin film (≈900 nm thickness) on Si 100 substrate with cut insulating channels for required thin-film geometry.

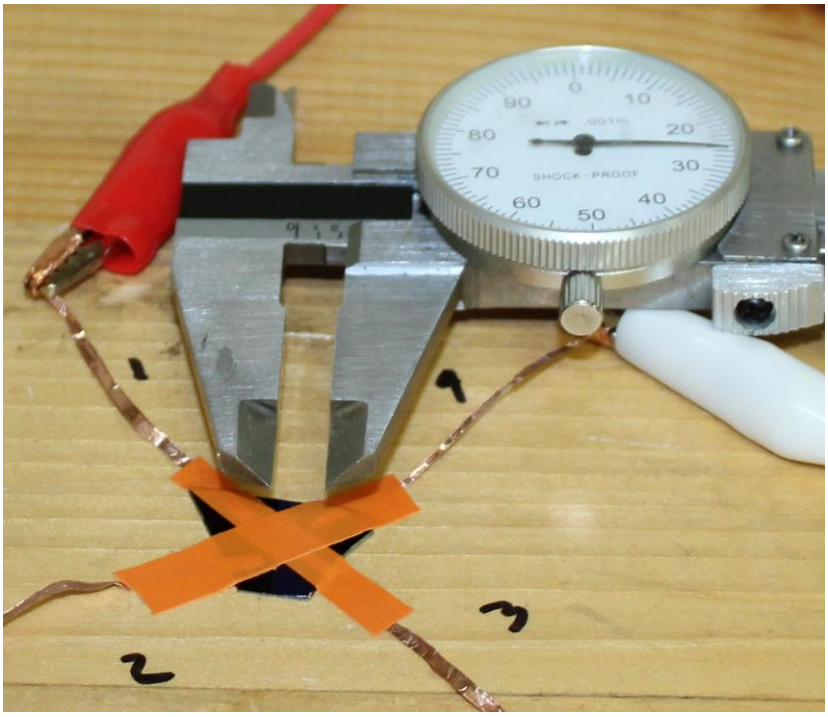

Figure 5.8 – a 4 terminal set up for Hall Voltage measurement as per NIST

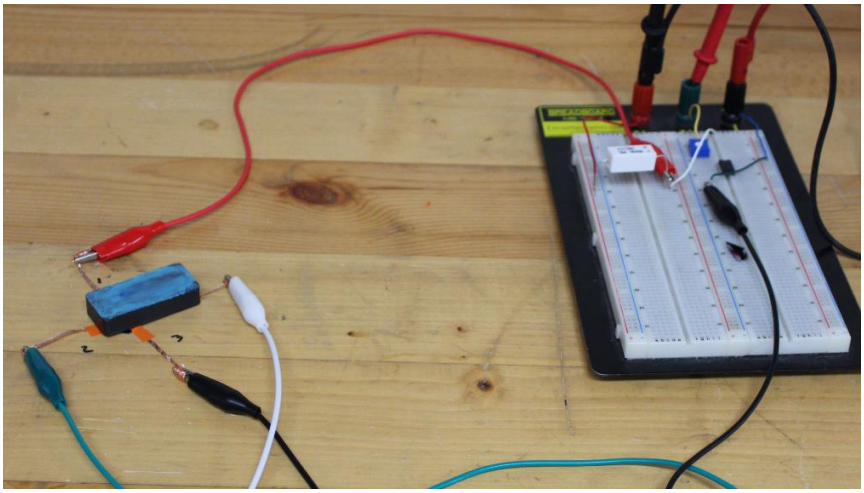

Figure 5.9 - Hall set up with a 300 Ohm current limiting resistor

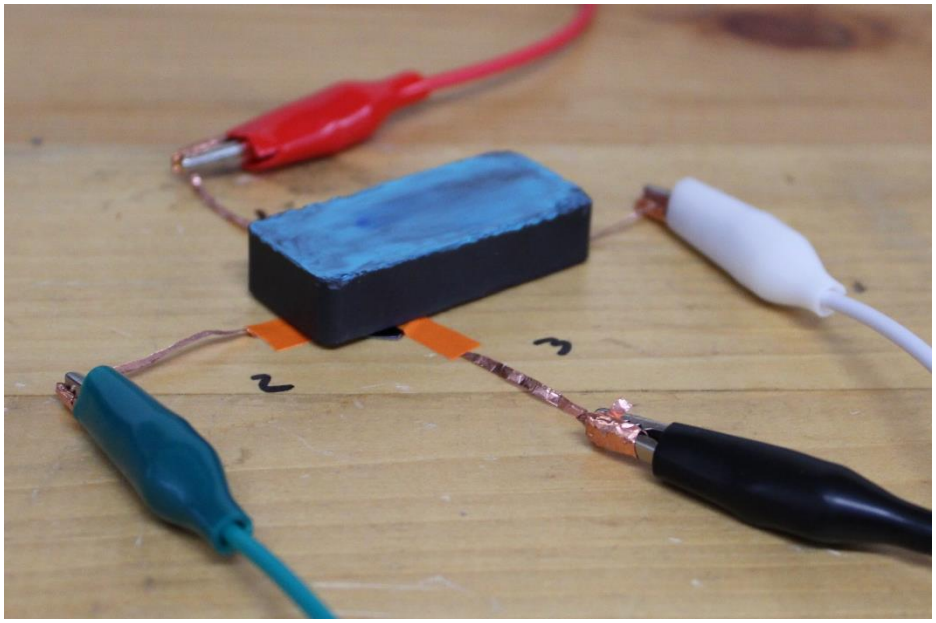

Figure 5.10 - Off the shelf magnet (900 Gauss) used for Hall measurement.

The Hall experiment set up requires the 4-port set up not only to provide a supply and measure the carrier deflection from the Hall Voltage, but it also requires a rotation of the 4 ports as to provide a basis for error correction. This also permits us to check whether the mobility is isotropic or if there is some rectification through the sample. Table 1 shows the data from the experiment performed on a sample with an approximate thickness of 900 nm (this is the sample in figures 5.7 & 5.8).

Table 5.2 - Hall Experiment Data

Measurement without Magnetic Field				
Current	Amperes	Potential	Volts	Resistance [Ohms]
I21	4.69E-04	V34	4.00E-04	8.53E-01
I12	8.72E-04	V43	2.00E-04	2.29E-01
I32	4.53E-03	V41	5.00E-04	1.10E-01
I23	4.66E-03	V14	5.00E-04	1.07E-01
I43	2.92E-03	V12	3.00E-04	1.03E-01
I34	6.03E-04	V21	3.00E-04	4.97E-01
I14	1.68E-03	V23	4.00E-04	2.39E-01
I41	1.34E-03	V32	1.00E-04	7.46E-02

Table 1 - Continued

Measurement with magnetic field						
	Current	Amps	Potential	Volts		
posB	I13	1.31E-03	V24p	4.20E-03	Vc =	5.20E-03
	I31	7.37E-06	V42p	2.40E-03	Vd =	3.90E-03
	I42	1.36E-03	V12p	2.40E-03	Ve =	4.20E-03
	I24	1.14E-03	V31p	2.30E-03	Vf =	3.70E-03
negB	I13	6.57E-03	V24n	-1.00E-03		
	I31	6.32E-03	V42n	-1.50E-03		
	I42	6.57E-03	V12n	-1.80E-03		
	I24	6.03E-04	V31n	-1.40E-03		

Set the error limit $\delta = 0.0005$, corresponding to 0.05 %

Calculate the initial value of z_1, or $z_o = 2\ ln(2)/[\pi(R_A + R_B)]$

Calculate the i^{th} iteration of $y_i = 1/\exp(\pi\, z_{i-1} R_A) + 1/\exp(\pi\, z_{i-1} R_B)$

Calculate the i^{th} iteration of z_i where

$$z_i = z_{i-1} - [(1-y_i)/\pi] / [R_A/\exp(\pi\, z_{i-1} R_A) + R_B/\exp(\pi\, z_{i-1} R_B)]$$

When $(z_i - z_{i-1})/z_i$ is less than δ, stop and calculate the sheet resistance $R_S = 1/z_i$

The resistivity ρ is given by $\rho = R_S d$, where d is the thickness of the conducting layer

Figure 5.11 - Algorithm for error correction in Hall effect measurement as per NIST

```
# this is a redundant calculation to reduce error due to measurement
# the routine takes 2 data inputs, Ra and Rb
Ra = 0.421
Rb = 0.133

errMax = 0.0005 # state minimal error allowed per unit
err = 1000000   # initialize error at 1e6
pi = 3.1416
z0 = math.log(2)/(pi*(Ra+Rb))*2
y0 = 1/(math.exp(pi*z0*Ra)) + 1/(math.exp(pi*z0*Rb))
n = 0
z = [z0]
y = [y0]

while (errMax < err):
    z.append(0)
    n = len(z)-1
    zn = z[n-1] - ((1-y[n-1])/pi)/((Ra/math.exp(pi*z[n-1]*Ra) + Rb/math.exp(pi*z[n-1]*Rb)))
    z[n] = (zn)
    yn = 1/(math.exp(pi*z[n]*Ra)) + 1/(math.exp(pi*z[n]*Rb))
    y.append(yn)
    err = (z[n]-z[n-1])/z[n-1]

    # return "%.1f" % n

Rs = 1/z[n]
```

Figure 5.12 - Python implementation of the sheet resistivity and error correction calculations for Hall measurement

RESULTS AND DISCUSSION

The Hall Voltage measurement was performed on a c-BN thin film. [25] The deposition was done at 6mT, 600℃, 6Ar/9N_2, for 18 Hr. The voltage polarity measurement indicates that holes are the majority charge carrier, effectively making this a sample of p-type conductivity, or a p-type semiconductor. The measurement and computation yield values for semiconductor type, majority charge carrier concentration p, majority carrier mobility μ_p, and sample conductivity σ as follows.

$$p = 7.89 \times 10^{20} cm^{-3}$$

$$\mu_p = 3.16 \times 10^{-2} cm^2 V^{-1} s^{-1}$$

$$\sigma = 1.97 \times 10^6 S/m$$

Figure 5.12 contains the python code implementation of the Sheet resistivity measurement and error correction that yields the values above.

The sample is conductive and, given that the resistivity of the substrate is much higher, in order of magnitude, it is safe to assume that all the conductive behavior comes from the thin film or a combination of the interaction of the thin film and the substrate. The known large grain size of the deposited films indicates an accumulation of stress [29][30][35] in the grains, this stress contributes to the electrical conductivity by overcoming the WBG $Eg = 6.4\ eV$ through the piezoelectric effects. It is this grain formation that contributes to both, the high carrier concentration and low mobility. The mobility is affected by having the wave packets encounter many discontinuities across any direction of travel. This thin film, however, consists of the cubic phase of BN, and it is therefore thermochemically inert in very aggressive environments. This

confirms the material as a good candidate for applications such as sensing and high-power electronics and sensing applications.

The results are in agreement with in order of magnitude, the theoretical calculation possible due to the SEM and AFM imaging. The justification for this is as follows. When the charge carrier moves freely in a periodic crystal the wave function is well represented by a traveling wave packet, until it approaches a discontinuity or a potential step. Every grain boundary is taken seen by the traveling wave packet as a collision, or a potential step, as is commonly seen from the point of view of quantum mechanics. At this potential the wave is either transmitted or reflected, depending on the boundary and the energy of the wave packet. Previous studies show different values, it is assumed in this work that this is due to thin film grain quality.

Scanning Electron Microscope imaging shows the smallest grain size formation of c-BN for given sputtering gas ratio Ar:N_2 = 6:9 sccm, a deposition is carried through 18Hrs, at 100W, and 600℃ this produces a film thickness of 900nm. Depending on the application, this is a better-quality, with grain size formation of $\approx 10\ nm$, in addition to not having formed grains all throughout the thin film (smooth surface) with suggests a higher hole mobility. A much lower carrier concentration is expected of this sample due to much lower accumulated stress in the grains and crystal formation in general. To further reduce the grain size and improve the thin film quality, the sample is annealed at a temperature of 800℃ for 9hrs. The resistivity, majority charge carrier concentration, and carrier mobility are determined by the Hall Voltage measurement.

FUTURE WORK

Although the samples deposited achieve high conductivity when compared to the expected high resistivity due to the WBG, the improvement in thin-film quality could contribute to better match between theory and experiment, i.e. decreasing the charge carrier concentration by reducing the piezoelectric stress caused by high density grain formation. This would achieve the low charge carrier concentration and lower the electric conductivity.

The current film can be used for high power devices, since it has a high charge carrier concentration and a WBG, and a low mobility as a result. These parameters can be paired with other known properties of c-BN, such as thermochemical stability, mechanical stress resistance, and fair thermal conductivity.

REFERENCES

[1] K. Yuge, "Prediction of superhard cubic boron-carbon nitride trhough first principles," *Journal of Physics: Condensed Matter,* no. doi:10.1088/0953-8984/21/41/415403, 2009.

[2] e. a. Yingcai Fan, "Electronic Properties of BN/C nanotube heterostructure," *JOURNAL OF APPLIED PHYSICS,* no. DOI:10.1063/1.3383058, 2010.

[3] e. a. Y.N. Zhao, "Preparation of c-BN films by RF sputtering and the relation of BN phase formation to the substrate bias and temperature," *Thin Film Solids, Elsevier Science,* 1998.

[4] e. a. Wang Fang, "Microstructure and Piezoelectric Properties pf c-BN Nano-Films Depositedon Si by RF Sputtering for Piezoelectric Devices," in *International Nanoelectronics Conference,* 2013.

[5] e. a. W.S. Tan, "High temperature performance of AlGaN/GaN HEMTs on Si Substrates.," *Solid-Sate Electronics,* no. DOI: 10.1016/j.sse.2006.02.008, 2006.

[6] e. a. W. S. Tan, "High temperature performance of AlGaN/GaN HEMTs on Si substrates," *Solid S*

[7] e. a. Vipin Joshi, "A Comprehensive Computational Modeling Approach for AlGaN/GaN," *IEEE Transactions on Nanotechnology,* no. DOI10.1109/TNANO.2016.2615645 , November 2016.

[8] e. a. V. N. Brudnyi, "THE CHARGE NEUTRALITY LEVEL AND THE FERMI LEVEL PINNING IN A3N (BN, AlN, GaN, InN) NITRIDES," *Russian Physics Journal,* vol. 51, no. 12, 2008.

[9] e. a. Tuan Quy Nguyen, "Fabrication and Characterization of BN/AlGaN/GaN metal-insulator-semiconductor heterojunction field-effect transistors with sputtering-deposited BN gate dielectric.," *Phys Status Solidi,* p. DOI10.1003/pssc.201300390, 2013.

[10] V. Silitsky, "Si - Silicon," Ioffe Institute, [Online]. Available: http://www.ioffe.ru/SVA/NSM/Semicond/Si/. [Accessed 21 10 2018].

[11] V. Siklitsky, "BN - Boron Nitride," Ioffe Institute, [Online]. Available: http://www.ioffe.ru/SVA/NSM/Semicond/BN/. [Accessed 21 10 2018].

[12] e. a. Shoon Jeong, "Effects of Nitrogen Partial Pressure During RF Magnetron Sputtering on the Crystal Structure and Growth Rate of c-BN Films".

[13] e. a. Ruoxi Wang, "A theoretical study of silicon-doped boron nitride nanotubes serving as a potential chemical sensor for hydrogen cyanide," *Nanotechnology,* no. doi:10.1088/0957-4484/20/50/505704.

[14] e. a. R. Riane, "Pressure dependance of elecctronic and optical proeprties of Zinc-blende GaN, BN and their B0.25Ga0.75N allow," *Physica B,* no. doi:10.1016/j.physb.2009.10.038, 2010.

[15] S. A. R. Moradian, "Magnetism in defected single-walled boron nitride nanotubes," *A LETTERS JOURNAL EXPLORING THE FRONTIERS OF PHYSICS,* no. doi: 10.1309/0295-507/83/17007, 2008.

[16] e. a. Michael O. Atambo, "QMC and phonon study of super-hard cubic boron carbon nitride," *Materials Research Express,* no. doi:10.1088/2053-1591/2/10/105902, 2015.

[17] e. a. M.A. Djouadi, "Deposition of boron nitride films by PDV methods: transition from h-BN to c-BN," *Surface and Coatings Technology,* no. DOI:10.1016/jsurfcoat.2003.10.156, 2004.

[18] e. a. M. Chibarov, "Boron nitride: A new photonic material," *Physica B,* no. http://dx.doi.org/10.1016/j.physb.2013.10.068, 2014.

[19] e. a. L. M. Cao, "Boron nitride nanotube branched nanojunctions," *Nanotechnology,* no. doi:10.1088/0957-4484/18/15/155605, 2007.

[20] R. H. W. Jr., "Borazon.," *Science, New Series,,* vol. 125, p. 437, March 1957.

[21] e. a. Jin-Hyo Boo, "MOCVD of BN and GaN thin films on silicon: new attempt of GaN growth with BN buffer layer," *Journal of Crystal Growth,* 1998.

[22] e. Jianping Long, "Predicting crystal structures and physical properties of novel superhard p-BN under pressure via firs-principles investigation," *Journalof Alloys and Compounds,* no. http://dx.doi.org/10.1016/jallcom.2015.04.229, 2015.

[23] e. a. Hui Pan, "Boron nitride and carbon-wall hetero-nanotubes: first-principles calculation of electronic-properties," *Nanotechnology,* no. doi:10.1088/0957-4484/199/095707, 2008.

[24] e. a. Hui Hu, "Protection of BN for MgB2 Films Against Degradation in Water," *IEEE TRANSACTION ON APPLIED SUPERCONDUCTIVITY,* no. DOI 10.1109/TASC.2016.2565599, 2016.

[25] e. a. Hanson Cheng, "First principles calculation of thermodynamics for semiconductor alloys," *Chemical Physics Letters,* no. doi:10.1016/j.cplett.2005.06.110, 2005.

[26] J.-M. L. a. J. Haines., "The search for super-hard materials.," *Elsevier Science Ltd.,* vol. Endeavour Vol. 21(3), 1997.

[27] V. L. S. a. E. Gregoryanz, "Synthesis of superhard materials," *Materials Today,* November 2005.

[28] e. a. G. Liu, "Selective Gas Sensing With h-BN Capped MoS2 Heterostructure Thin-Film Transistors.," *IEEE Electron Device Letters,* no. DOI: 10.1109/LED.2015.2481388, 2015.

[29] e. a. Fang Wang, "Microstructure and Nanometer Scale Piezoelectric Properties of c-BN Thin Films With Cu Buffer Layer by Piezoresponse Force Microscopy," *IEEE TRANSACTIONS ON NANOTECHNOLOGY,* no. DOI 10.1109/TNANO.2013.2277599, 2014.

[30] e. a. F. Menacer, "Modeling of Boron Nitride-based Nanotube biological Sensor using Neural Networks," in *International conference on Sciences and techniques of Automatic Control &computer engineering*, Tunisia, 2016.

[31] J. B. Durga Misra, "Crystal Radio Detector ("Cat's Whisker"): the First WirelessDevice," *IEEE Circuits and Devices Magazine,* March 2001.

[32] e. a. D.R. McKenzie, *Diamond Relat. Mater. 2,* no. 970, 1993.

[33] e. a. D.J. Kester, *J. Appl. Phys.*, no. 504, p. 72, 1992.

[34] e. a. D. N. Talwar, "Elastic, structural, conding, and defect properties of zinc-blende BN, AlN, GaN, InN and their alloys," *Materials Science Engineering B,* vol. 90, pp. 269-277, 2002.

[35] e. a. Chen Xi-ming, "Research on the piezoelectric response of cubic and hexagonal boron nitride films," *Optoelectronics Letters,* vol. 8, no. DOI 10.1007/s11801-012-1177-1, 2012.

[36] H. C. CASEY, DEVICES FOR INTEGRATED CIRCUITS, SILICON AND III-V COMPOUND SEMICONDUCTORS, JOHN WILEY AND SONS, INC, 1999.

[37] V. N. Brudnyi, "BN, AlN, GaN, InN: CHARGE NEUTRALITY LEVEL, SURFACE, INTERACES DOPING," *Russian Physics Journal,* no. DOI 10.1007/s11182-017-1035-5, 2017.

[38] e. a. B.X. Du, "Thermal Conductivity and Arcing Resistance of Micro or Hybrid BN Filled Polyethylene under Pulse Strength.," *IEEE Transactions on Dielectrics and Electrical insulators,* no. DOI: 10.1109/TEDI.2016.005522, October 2016.

[39] R. F. D. I.-V. N. f. E. a. O. Applications, "III-V Nitrides for Electronic and Optoelectronic Applications".

[40] A. K.-V. S. W. G. a. C. J. P. Alexander V. Naumkin, "NIST X-ray Photoelectron Spectroscopy Database," NIST, [Online]. Available: https://srdata.nist.gov/xps/ElmComposition.aspx. [Accessed December 2017].

[41] V. R. e. al., "Correlation of boron and nitrogen contents witht he flux of energetic Ar+ ions at the substrate during the deposition of BN coatings by RF magnetron sputtering," *Surface and Coatings Technology,* pp. 275-280, 1997.

[42] R. K. e. al., "Complex XRD microstructural studies of hard coatings applied to PVD-deposited TiN films," *Thin Solid Films,* no. 268, pp. 72-82, 1995.

[43] N. .. F. e. al., "Different nanostructures identified in boron nitride thin films grown on Si (100) by rf magnetron sputtering," *Diamond & Related Materials,* vol. 18, no. doi:10.1016/j.diamond.2008.07.008, pp. 6-12, 2009.

[44] M. B. e. M. e. al., "Structure investigation of BN films grown by ion-beam-assisted deposiyion by means of polarized IR and Raman spectroscopy," *Surface Coatings and Technology,* vol. 116, no. 119, pp. 93-99, 1999.

[45] M. M. e. al., "Microstructure study of BN nano-composites using XRD and HRTEM," *Z Krystallogr. Suppl.* , vol. 27, no. DOI 10.1524/zksu.2008.0007, pp. 45-52, 2008.

[46] G. D. e. al., "Synthesis and tayloring of GaN nanocrystals at room temperature by RF magnetron sputtering," *Radiation Effects and Deffects in Solids,* vol. 167, no. 9, pp. 659-665, 2012.

[47] G. Abadias, "Stress and preferred orientation in nitride-based PVD coatings," *Surface and Coatings Technology,* no. 2002, pp. 2223-2235, 2008.

[48] "Professional Plastics," [Online]. Available: http://www.professionalplastics.com/professionalplastics/ThermalPropertiesofPlasticMaterials.pdf. [Accessed 21 10 2018].

[49] A Rastogi, et. al. STPS Technologies Ltd. IEEE, "Productivity Challenges in PVD Processing in 300mm Pilot Lines for Power Semiconductors," 2015.

BIBLIOGRAPHICAL SKETCH

Jesús A. Valladares González, born in San Nicolas de los Garza, N.L. México. Received a Bachelor of Science in Electrical Engineering from the University of Texas Pan American (UTPA) in December 2013, and a Master of Science from UTRGV on December 2018. Jesus performed Medium Voltage Power Line Design as an Engineer for American Electric Power, he is currently an Electron Beam Operator for Scantech Sciences. He has specialized training in Fault Current Protection, Volt-Var Regulation, and Protective Device Coordination, S-Band High Power Pulse Modulators, Ultra High Vacuum Systems. Jesus is a certified EIT in the State of Texas and is currently pursuing professional licensure. Jesus's graduate work is part of his interest in the field of semiconductor devices and the applications of quantum mechanics. Jesus has interests in Physics and Engineering. His practice includes system design and specification, construction and construction management, equipment testing and troubleshooting.

Currently resides at 1917 Cornell Ave. McAllen, TX. And can be reached at vallagon_89@hotmail.com.